Two–Photon Oxygen Sensing with Quantum Dot–Porphyrin Conjugates

Christopher M. Lemon[a,b], **Elizabeth Karnas**[a], **Moungi G. Bawendi**[a], and **Daniel G. Nocera**[b]

[a]Department of Chemistry, Massachusetts Institute of Technology, 77 Massachusetts Avenue, Cambridge, MA 02139

[b]Department of Chemistry and Chemical Biology, 12 Oxford Street, Harvard University, Cambridge, MA 02138

Abstract

Supramolecular assemblies of a quantum dot (QD) associated to palladium(II) porphyrins have been developed to detect oxygen (pO_2) in organic solvents. Palladium porphyrins are sensitive in the 0–160 torr range, making them ideal phosphors for *in vivo* biological oxygen quantification. Porphyrins with *meso* pyridyl substituents bind to the surface of the QD to produce self–assembled nanosensors. Appreciable overlap between QD emission and porphyrin absorption features results in efficient Förster resonance energy transfer (FRET) for signal transduction in these sensors. The QD serves as a photon antenna, enhancing porphyrin emission under both one– and two–photon excitation, demonstrating that QD–palladium porphyrin conjugates may be used for oxygen sensing over physiological oxygen ranges.

INTRODUCTION

Generating metabolic profiles of tumors provides a spatiotemporal map of the concentration of key species to assess and quantify tumor growth, metabolism and response to therapy. Because the tumor microenvironment is characterized by acidity and hypoxia,[1] the concentration of protons and oxygen are important indicators of tumor health.[2] Understanding how these two parameters change as a function of disease progression is critical to develop novel targeted therapeutics such as antiangiogenic agents, which can engender normalization of the leaky, distended, and tortuous tumor vasculature.[3] Upon normalization, blood flow, oxygen levels, and drug distribution are increased; this represents an opportunity to treat the tumor with a substantial dose of chemotherapeutics to have a superior impact on tumor progression.[4] However, the normalization process must be efficiently monitored so that doses of chemotherapeutics can be timed appropriately to have a maximal effect on tumor viability. To address this challenge, new non–invasive sensors must be developed that are small enough to penetrate into the tumor and monitor dynamic changes with high resolution.[5] To this end, we have developed self–referencing pH sensors[6–8] and a high–pressure (160–760 torr) oxygen sensor[9] to probe biological

microenvironments. Herein, we report a low–pressure (0–160 torr) oxygen sensor that covers the oxygen concentration range of the hypoxic tumor environment.

Fluorescent semiconductor quantum dots (QDs) have high quantum yields, photostability, narrow emission bands, and broad excitation profiles,[10] rendering them ideal scaffolds for constructing optical biosensors.[11–13] By attaching an analyte–sensitive fluorophore to the QD, Förster resonance energy transfer (FRET) may be exploited as a means of signal transduction.[14–16] Additionally, QDs exhibit high two–photon absorption cross–sections (σ_2 ~10^4 Göppert–Mayer, 1 GM = 10^{-50} $cm^4 \cdot s/photon$),[17–19] making them attractive fluorophores for multiphoton imaging. Near–IR excitation and detection (600–1000 nm) in the so–called therapeutic window allows for imaging with minimal background signal from cellular autofluorescence.[20] This spectral window is readily accessed using two–photon excitation. This imaging technique is nondestructive to tissue and provides high–resolution images of live tissue at depths of several hundred microns with submicron spatial resolution.[21,22] Thus, QDs offer a versatile platform on which to build supramolecular oxygen sensing assemblies.

Many oxygen sensitive phosphors have been reported in the literature using osmium,[9] iridium,[23] and ruthenium[24] polypyridine complexes as well as pyrene.[25] Platinum and palladium porphyrins are especially well–suited for O_2 sensing applications due to their strong room temperature phosphorescence in the 650–800 nm range and long (~10^2 μs) phosphorescence lifetime.[26] Most oxygen chemosensors heretofore have relied on the immobilization of these porphyrins in polymer matrices,[26–28] on solid surfaces,[26,29] or in mesoporous silica.[26,30] Commercial palladium porphyrins (Oxyphor R2) and benzoporphyrins (Oxyphor G2), which are available as water–soluble glutamate dendrimers, have also been used for oxygen sensing in solution.[31]

The exceptionally long phosphorescence lifetimes of palladium porphyrins make them ideal for oxygen sensing in the biologically relevant 0–160 torr range. The heavy metal Pd promotes rapid intersystem crossing to produce the long–lived triplet state. Molecular oxygen (a ground state triplet) deactivates this excited state efficiently through collisional quenching, as dictated by Stern– Volmer kinetics. By monitoring the intensity or lifetime of the triplet excited state of the Pd porphyrin, the amount of oxygen may be quantified.[32] However, porphyrins alone have prohibitively low two–photon absorption cross–sections (σ_2 = 1–25 GM for free–base tetraphenylporphyrin),[33] and thus an ideal oxygen sensor using Pd porphyrins combines the oxygen–sensitive properties of porphyrins with an efficient two–photon antenna. In this regard, coumarin dyes have served as two–photon antenna for covalently attached Pd or Pt porphyrins.[34–37] Herein, we expand this approach by using a QD as the two–photon antenna.

The porphyrin–QD construct shown in Figure 1 is prepared by self–assembly, promoted by binding of Pd porphyrins with *meso*– pyridyl substituents (compounds **1–3**) to the surface of a QD. In this sensing scheme, the QD is irradiated with two–photon excitation and energy is transferred via FRET to excite the Pd porphyrin, which is quenched by molecular oxygen; the extent of quenching is proportional to the amount of oxygen. Since the QD is unaffected by oxygen, its emission may serve as an internal standard to afford a ratiometric oxygen sensor by monitoring the QD:porphyrin emission intensity.

The system shown in Figure 1 offers several new advantages for O_2 sensing. First, the self–assembling process allows for facile construction of a nanosensing construct. Second, QDs are among the most efficient two–photon chromophores, exhibiting absorption cross–sections that are 1000–fold greater than common organic dyes (σ_2 ~ 10^4 GM for QDs versus σ_2 = 20 GM for Coumarin–343).[35] Third, the photophysical properties, namely the emission

wavelength, of QDs are tunable,[10] enabling optimized spectral overlap between Pd porphyrin and QD, thus maximizing FRET efficiency. Fourth, several porphyrins are associated to a single two–photon QD antenna, giving a sizable porphyrin response on a per sensor basis. Fifth, the insensitivity of QD emission to O_2 establishes a ratiometric signal response. Finally, the construct exhibits greatest response over the biologically important 0– 160 torr O_2 pressure range.

EXPERIMENTAL

Materials

The following chemicals were used as received: hexanes, diethylether (Et_2O), anhydrous inhibitor–free tetrahydrofuran (THF), dichloromethane (CH_2Cl_2), toluene, acetonitrile (MeCN), methanol (MeOH), anhydrous methanol (MeOH), ethanol (EtOH), ethyl acetate (EtOAc), 2– mercaptopyridine, isonicotinoyl chloride hydrochloride, nicotinoyl chloride hydrochloride, pyrrole, 4–pyridinecarboxaldehyde, 3– pyridinecarbox-aldehyde, benzaldehyde, methyl 4–formylbenzoate, indium(III) chloride ($InCl_3$), sodium hydroxide (NaOH) beads, ethyl magnesium bromide 1 M solution in THF (EtMgBr), bromine (Br_2), 1,8–diazabicyclo[5.4.0]undec–7–ene (DBU), magnesium bromide ($MgBr_2$), tris(2,2′– bipyridyl)dichlororuthenium(II) hexahydrate ([Ru(bpy)]Cl_2), 2′,7′–dichlorofluorescein (fluorescein 27), trifluoroacetic acid (TFA), triethylamine (NEt_3), 2,3–dichloro–5,6– dicyano–1,4– benzoquinone (DDQ), and sodium borohydride ($NaBH_4$) from Sigma– Aldrich; sodium bicarbonate ($NaHCO_3$), sodium sulfate (Na_2SO_4), ammonium chloride (NH_4Cl), ammonium sulfate (($NH_4)_2SO_4$), and sodium chloride (NaCl) from Mallinckrodt; potassium carbonate (K_2CO_3) and Celite 512 from Fluka; palladium(II) acetylacetonate (Pd(acac)$_2$) and ytterbium(III) triflate (Yb(OTf)$_3$) from Strem; benzoyl chloride from J. T. Baker; pyridine from EMD; silica gel 60Å 230–400 mesh ASTM from Whatman; and chloroform–*d* ($CDCl_3$) from Cambridge Isotope Labs. Nitrogen and argon gases (Airgas) were passed over a Drierite column prior to use. Cadmium selenide core/shell quantum dots (518 nm emission, QD Vision) were twice precipitated from toluene using EtOH and redissolved in toluene prior to use. The following compounds were prepared according to literature procedures or slight modifications thereof: 5–(3– pyridyl)dipyrromethane (**S1**),[38] *S*–2–pyridyl nicotinothioate (**S2**),[39,40] 5–phenyldipyrromethane (**S3**),[41,42] *S*–2–pyridyl benzoylthioate (**S4**),[39,43] 5–(4–methoxycarbonylphenyl) dipyrromethane (**4**),[41,42] *S*–2– pyridyl isonicotnothioate (**5**),[39,40] 1– isonicotinoyl–5–(4–pyridyl) dipyrromethane (**7**),[39,40] 1–nicotinoyl–5–(3–pyridyl)-dipyrromethane (**8**),[39,40] 1–benzoyl–5– phenyldipyrromethane (**9**),[39,40] 1,9–dibenzoyl–5– phenyldipyrromethane (**10**),[38] and 5–(4–pyridyl)dipyrromethane (**12**).[38] Exact procedures for the preparation of these compounds and ^{1}H NMR are provided in the Supporting Information.

1–Isonicotinoyl–5–(4–methoxycarbonylphenyl)dipyrro–methane (6)

This compound was prepared using a procedure similar to that used for other 1–acyl dipyrromethanes,[39,40] with minor modifications including the addition of acylating reagent as a solid in one portion rather than a homogenous solution. In an oven–dried flask, 1.89 g 5–(4–methoxycarbonylphenyl)dipyrromethane (**4**)[41,42] (6.74 mmol) was dissolved in 15 mL anhydrous THF under an argon atmosphere to afford a tan solution. 17 mL EtMgBr (1 M solution in THF) was then slowly added and the resultant dark brown solution was stirred at room temperature for 10 min. The solution was cooled to −78 °C in a dry ice/acetone bath and 1.50 g (6.94 mmol) *S*–2–pyridyl isonicotinothioate (**5**)[39,40] was added in one portion; the resultant mixture was stirred at −78 °C for 1 h. The solution was warmed to room temperature and stirred for an additional 3 h. Saturated NH_4Cl was added and the product was extracted with EtOAc. The combined organics were washed with water and brine then dried over Na_2SO_4. Solvent was removed by rotary evaporation to afford a brown oil. The

crude reaction mixture was loaded onto a silica gel column packed with ethyl acetate. The product (second band, which turns yellow– orange upon Br_2 staining on TLC) was eluted with 100% EtOAc. After solvent removal, the oily brown residue was dissolved in a minimal amount of EtOAc and subsequently precipitated with a large excess of hexanes and the resultant solid was collected on a frit and washed with hexanes to afford 1.67 g (64.2% yield) of the title compound as a tan solid. ^{1}H NMR (500 MHz, $CDCl_3$) δ = 3.92 (s, 3H), 5.61 (s, 1H), 5.97 (m, 1H), 6.08 (m, 1H), 6.19 (m, 1H), 6.76 (m, 1H), 6.81 (m, 1H), 7.30 (m, 2H), 7.63 (m, 2H), 8.01 (m, 2H), 8.04 (bs, 1H), 8.77 (m, 2H), 9.56 (bs, 1H).

5–(4–Methoxycarbonylphenyl)–10,15,20–tris(4–pyridyl)-porphyrin (1-H2)

This compound was prepared using a microwave–mediated [2+2] condensation.[40] In a 10 mL microwave tube, 69 mg (0.21 mmol) 1–isonicotinoyl–5–(4–pyridyl)dipyrromethane (**7**)[39,40] and 76 mg (0.20 mmol) 1–isonicotinoyl–5–(4–methoxycarbonylphenyl)dipyrromethane (**6**) were dissolved in 4 mL toluene to afford a dark brown–black suspension. The suspension turned red after the addition of 0.6 mL DBU (0.6 g, 4 mmol), and was stirred for 5 min at room temperature. $MgBr_2$ (420 mg, 2.3 mmol) was added and an additional 1 mL toluene was added to rinse the walls of the tube. The resultant orange–brown suspension was placed in a microwave reactor (CEM Discover) and irradiated at 115 °C for 2 h. The reaction mixture was transferred to a flask, dissolved in THF, and the solvent was removed by rotary evaporation. The residue was dissolved in EtOAc, washed with water, and brought to dryness under rotary evaporation. The magnesium porphyrins of the crude reaction mixture were demetallated by dissolving the residue in 10 mL CH_2Cl_2 and adding 0.2 mL TFA (0.3 g, 2.6 mmol); the resulting green solution was stirred at room temperature for 30 min. Then 0.4 mL NEt_3 (0.3 g, 2.9 mmol) was added and the reaction mixture was washed with water and brine, dried over Na_2SO_4, and brought to dryness. The residue was loaded onto a silica gel column and eluted with EtOAc. After removal of the *trans*–A_2B_2 product, the solvent was changed to 4% MeOH in EtOAc to give 15 mg (11% yield) of the title compound. ^{1}H NMR (500 MHz, $CDCl_3$) δ = – 2.90 (bs, 2H), 4.12 (s, 3H), 8.16 (m, 6H), 8.30 (m, 2H), 8.47 (m, 2H), 8.82–8.89 (bm, 8H), 9.06 (m, 6H).

5,10–Diphenyl–15,20–bis(3–pyridyl)porphyrin (2-H2)

This compound was prepared using a microwave–mediated [2+2] condensation.[40] In a 10 mL microwave tube, 60 mg (0.18 mmol) 1– nicotinoyl–5–(3–pyridyl)dipyrromethane (**8**)[39,40] and 60 mg (0.18 mmol) 1–benzoyl–5–phenyldipyrromethane (**9**)[39,40] were dissolved in 4 mL toluene to afford a dark brown–black suspension. After the addition of 0.6 mL DBU (0.6 g, 4.0 mmol), the suspension became red and was subsequently stirred for 5 min. $MgBr_2$ (453 mg, 2.46 mmol) was added and 1 mL toluene was added to rinse the solids down the tube. The resultant orange– brown suspension was placed in a microwave reactor (CEM Discover) and irradiated at 115 °C for 2 h. The reaction mixture was transferred to a flask, dissolved in THF, and the solvent was removed by rotary evaporation. The residue was dissolved in ethyl acetate, washed with water and brine, dried over Na_2SO_4, and brought to dryness. The crude reaction mixture was purified on a silica gel column using ethyl acetate as the eluent to remove the first major band, Mg(TPP). The solvent was then switched to 5% MeOH in EtOAc to elute the desired product, which moved as the second fluorescent band on the column. The A_4 complex with four 3–pyridyl groups remained at the top of the column and was not isolated. The Mg complex was demetallated by dissolving the solid in 10 mL CH_2Cl_2 and adding 0.2 mL TFA (0.3 g, 2.6 mmol); the resulting green solution was stirred at room temperature for 30 min after which 0.4 mL NEt_3 (0.3 g, 2.9 mmol) was added. The reaction mixture was washed with water and brine, dried over Na_2SO_4, and brought to dryness. The free–base porphyrin (27 mg, 24% yield) was used without further purification. ^{1}H NMR (500 MHz, $CDCl_3$) δ = −2.81 (bs, 2H), 7.75–7.81

(overlapping m, 6H), 7.79 (overlapping m, 2H), 8.22 (d, J = 6.1 Hz, 4H), 8.53 (d, J = 6.8 Hz, 2H), 8.80 (d, J = 4.7 Hz, 2H), 8.84 (s, 2H), 8.87 (s, 2H), 8.91 (d, J = 4.7 Hz, 2H), 9.06 (m, 2H), 9.46 (s, 2H).

5,10,15–Triphenyl–20–(4–pyridyl)porphyrin (3-H$_2$)

In an oven–dried flask, 90 mg 1,9–dibenzoyl–5–phenyldipyrromethane (**10**)[38] (0.21 mmol) was dissolved in 12 mL anhydrous THF and 4 mL anhydrous MeOH under a nitrogen atmosphere to give a brown solution. To this solution, 0.42 g NaBH$_4$ (11 mmol) was added and the resultant tan–orange mixture was stirred at room temperature for 1 h. Water was added to quench excess NaBH$_4$ and the product was extracted with CH$_2$Cl$_2$ and dried over K$_2$CO$_3$ to afford a solution of the corresponding dicarbinol (**11**). Since the dicarbinol is prone to decomposition, the solution was concentrated to near–dryness without heating. The residue was dissolved in 50 mL MeCN and 45 mg 5–(4– pyridyl)dipyrromethane (**12**)[38] (0.20 mmol) and 1.22 g Yb(OTf)$_3$ (2.0 mmol) were added; the resulting red solution was stirred at room temperature for 1 h all the while protected from light. DDQ (183 mg, 0.806 mmol) was added and the solution was stirred at room temperature for an additional 1 h. NEt$_3$ (2 mL, 1.6 g, 16 mmol) was added to the solution and stirred for an additional 30 min. Ethyl acetate was added and the reaction mixture was washed with water and brine, dried over Na$_2$SO$_4$, and brought to dryness. The product was purified on a silica gel column using EtOAc as the eluent to obtain 30 mg (24% yield) of the title compound. ^{1}H NMR (400 MHz, CDCl$_3$) δ = −2.80 (bs, 2H), 7.75–7.80 (m, 9H), 8.17 (m, 2H), 8.22 (m, 6H), 8.80 (d, J = 4.5 Hz, 2H), 8.86 (s, 4H), 8.90 (d, J = 4.7 Hz, 2H), 9.03 (m, 2H).

General procedure for palladium(II) metallation

In a 10 mL microwave tube, free–base porphyrin was dissolved in 3 mL pyridine and Pd(acac)$_2$ was added. An additional 1 mL of pyridine was added to rinse solids down the tube. The resultant solution was placed in a microwave reactor (CEM Discover) and irradiated at 180 °C for 20 min. The crude reaction mixture was filtered through a plug of Celite and rinsed with CH$_2$Cl$_2$; the collected orange filtrate was brought to dryness. The palladium complex was purified on a silica gel column to afford the product.

5–(4–Methoxycarbonylphenyl)–10,15,20–tris(4–pyridyl)-porphyrinopalladium(II) (1)

Following the aforementioned general procedure, 65 mg (0.10 mmol) of the free–base porphyrin **1-H$_2$** was treated with 175 mg (0.574 mmol) Pd(acac)$_2$. The compound was purified using a gradient of 0–10% MeOH in EtOAc as the eluent to give 39 mg (50% yield) of the title product. ^{1}H NMR (400 MHz, CDCl$_3$) δ 4.12 (s, 3H), 8.12 (m, 6H), 8.25 (m, 2H), 8.45 (m, 2H), 8.80 (d, J = 5.1 Hz, 2H), 8.82 (s, 4H), 8.83 (d, J = 5.0 Hz, 2H), 9.05 (m, 6H). Anal. Calcd. for (M+H)$^+$, M = C$_{43}$H$_{27}$N$_7$O$_2$Pd: 780.1339. Found: 780.1507. Elem. Anal. Calcd.: 66.20% C, 3.49% H, 12.57% N. Found: 66.14% C, 3.47% H, 12.53% N.

5,10–Diphenyl–15,20–bis(3–pyridyl)porphyrinatopalladium(II) (2)

Following the aforementioned general procedure, 16 mg of the free–base porphyrin **2-H$_2$** (0.03 mmol) was treated with 55 mg (0.18 mmol) Pd(acac)$_2$ then purified using EtOAc as the eluent to give 7 mg (32% yield) of the title product. ^{1}H NMR (500 MHz, CDCl$_3$) δ 7.72–7.80 (m, 8H), 8.16 (m, 4H), 8.48 (m, 2H), 8.76 (d, J = 5.1 Hz, 2H), 8.80 (d, J = 2.2 Hz, 2H), 8.84 (s, 2H), 8.87 (d, J = 5.1 Hz, 2H), 9.04 (m, 2H), 9.42 (m, 2H). Anal. Calcd. for (M+H)$^+$, M = C$_{42}$H$_{26}$N$_6$Pd: 721.1332. Found: 721.1335.

5,10,15–Triphenyl–20–(4–pyridyl)porphyrinatopalladium (II) (3)

Following the aforementioned general procedure, 30 mg (0.05 mmol) of the free–base porphyrin **3-H$_2$** was treated with 136 mg (0.446 mmol) Pd(acac)$_2$ then purified using

CH$_2$Cl$_2$ as the eluent to give 6 mg (17% yield) of the title product. ^{1}H NMR (500 MHz, CDCl$_3$) δ 7.72–7.80 (m, 9H), 8.13 (m, 2H), 8.16 (m, 6H), 8.75 (d, J = 5.1 Hz, 2H), 8.82 (s, 4H), 8.85 (d, J = 5.1 Hz, 2H), 9.02 (m, 2H). Anal. Calcd. for (M+H)$^+$, M = C$_{43}$H$_{27}$N$_5$Pd: 720.1380. Found: 720.1430.

Preparation of QD/porphyrin conjugates

Toluene stock solutions of each palladium porphyrin **1–3** (~100 μM) and QD (~10 μM) were prepared. The concentration of the QD stock solution was calculated using ε$_{350}$ = 4.34 × 10^5 M^{-1} cm^{-1}, as estimated using an empirical formula based on the first absorbance feature at 501 nm.[44] An aliquot of the QD stock (typically containing ~1 nmol of QDs) was dissolved in 4 mL of toluene; an appropriate volume of the porphyrin stock was then added to give 10 molar equivalents of porphyrin per QD. The resultant mixture was stirred overnight at room temperature to allow equilibration of the porphyrin to the QD surface, to furnish conjugates **QD1–QD3**.

Physical measurements

^{1}H NMR spectra were recorded at room temperature on a Varian Inova–500 or Bruker Avance–400 NMR spectrometer at the MIT Department of Chemistry Instrumentation Facility (DCIF) and internally referenced to the residual solvent signal (δ = 7.26 for CHCl$_3$ in CDCl$_3$).[45] Mass spectra were recorded on a Bruker micrO–TOF–QII LCMS ESI–TOF mass spectrometer in positive ion mode. All spectra were externally calibrated with sodium formate. Elemental analysis was performed by Complete Analysis Laboratories, Inc. (Parsippany, NJ). UV–vis absorption spectra were acquired using a Cary 5000 spectrometer. Steady–state emission and excitation spectra were recorded on a SPEX FluoroMax–3 spectrofluorimeter. Relative quantum yields of porphyrins (Φ_{sam}) were calculated using [Ru(bpy)$_3$]Cl$_2$ in MeCN as the reference according to the following equation,

$$\Phi_{sam} = \Phi_{ref} \left(\frac{A_{ref}}{A_{sam}} \right) \left(\frac{I_{sam}}{I_{ref}} \right) \left(\frac{\eta_{sam}}{\eta_{ref}} \right)^2 \quad (1)$$

where A is the measured absorbance, η is the refractive index of the solvent, I is the integrated emission intensity, and Φ_{ref} is the emission quantum yield of the reference. Φ_{ref} was taken to be 0.094 for a freeze–pump–thawed (FPT) sample of [Ru(bpy)$_3$]Cl$_2$ in MeCN.[46] The quantum yield of **QD** was similarly determined using fluorescein 27 in 0.1 M NaOH (Φ_{ref} = 0.87, η = 1.335)[47] as the standard. Porphyrin samples for quantum yield measurements, vacuum lifetime (τ_o) measurements, and evacuated steady–state emission spectra were prepared using three cycles of FPT to pressures below 10^{-5} torr.

Nanosecond time–resolved emission measurements of porphyrin lifetimes were acquired using a previously reported system.[48,49] Pump light was provided by the third harmonic (355 nm) of a Quanta–Ray Nd:YAG laser (Spectra Physics) operating at 10 Hz. The pump light was passed through a BBO crystal in an optical parametric oscillator (OPO), yielding a visible frequency that was tuned to 525 nm to excite **1–3** or 450 nm to excite the assemblies **QD1–QD3**. Excitation light was attenuated to 1–4 mJ per pulse for all experiments using neutral density filters. Emitted light was first passed through a series of long pass filters to remove excitation light and then entered a Triax 320 monochromator (Jobin Yvon Horiba) and was dispersed by a blazed grating (500 nm, 300 grooves/mm) centered at 685 nm. The entrance and exit slits of the monochromator were set to 0.36 mm in all experiments herein, corresponding to a spectral resolution of 4.5 nm. The signal was amplified by a photomultiplier tube (R928, Hamamatsu) and collected on a 1 GHz digital oscilloscope (9384CM, LeCroy); acquisition was triggered using a photodiode to collect scattered laser excitation light.

Femtosecond emission lifetime measurements were acquired using a Libra–F–HE (Coherent) chirped–pulse amplified Ti:sapphire laser system. Sub–100 fs laser pulses were generated in a mode–locked Ti:sapphire oscillator (Coherent Vitesse) which was pumped by a 5 W cw Coherent Verdi solid–state, frequency– doubled Nd:YVO$_4$ laser. The 80–MHz output was amplified in a regenerative amplifier cavity, pumped by a diode–pumped, frequency–doubled Nd:YLF laser (Coherent Evolution–30) to generate a 1 kHz pulse train with a wavelength of 800 nm. This was then used to pump an OperA Solo (Coherent) optical parametric amplifier (OPA), which is able to generate frequencies between 285 and 2600 nm. Excitation pulses of 450 nm were produced via fourth harmonic generation of the idler using a BBO crystal; the pulse power was attenuated to 2.5 mW at the sample. Emission lifetimes were measured on a Hamamatsu C4334 Streak Scope streak camera, which has been described elsewhere.[50] The emission signal was collected over a 140 nm window centered at 475 nm using 100, 50, 20, 10 or 5 ns time windows. Delays in the 100 ns time window were generated using a Hamamatsu C1097–04 delay unit, whereas a Stanford Research Systems DG535 delay generator was used to generate delays for the other time windows.

Two–photon emission spectra were generated using the aforementioned Libra–F–HE (Coherent) chirped–pulse amplified Ti:sapphire laser system. Excitation pulses of 800 nm were used directly from the Libra output; the pulse power was attenuated to 6 mW using neutral density filters and the beam was focused onto the sample using a 500 mm focal length lens. The emission spectrum was collected using a Hamamatsu C4334 Streak Scope streak camera in 140 nm windows centered at 500, 550 and 650 nm.

Two–photon lifetime measurements were performed using a previously described custom–built multiphoton laser–scanning microscope (MPLSM) in the Edwin L. Steel Laboratory at the Department of Radiation Oncology at Massachusetts General Hospital.[51] The MPLSM system was modified to enable lifetime measurements to be performed.[52] Sub–100 fs laser pulses were generated at a repetition rate of 80 MHz in a mode–locked Ti:sapphire oscillator (Spectra Physics Mai Tai HP), which was pumped by a 14 W cw Spectra Physics Millennia diode–pumped solid–state (DPSS) laser operating at 532 nm; the output of the Mai Tai laser was tunable over the 690–1040 nm range. The 850 nm laser output was adjusted using a 10RP52–2 zero–order half–wave plate (Newport) and a 10GL08AR.16 Glan–Laser polarizer (Newport) to attenuate the power to 700–800 mW for aerated samples and 400 mW for FPT samples. The beam was passed through a 350–50 KD*P Pockels cell (Conoptics) that amplified and switched the triggering pulses from a DG535 digital delay generator (Stanford Research Systems). The experimental square wave trigger pulse from the delay generator defined the repetition rate while a second delayed pulse defined the excitation pulse, which was 1.6 μs in duration for aerated samples and 15.36, 30.72, or 51.20 μs in duration for FPT samples. At the rejection site of the Pockels cell, a TDS–3052 oscilloscope (Tektronix) and photodiode were used to monitor the applied voltage and the optical response; the Pockels cell attenuated the beam to 10% of the incident power. The laser beam was directed into a custom–modified multiphoton microscope based on the Olympus Fluoview 300 laser scanner. The output beam from the scanner was collimated through a scan lens into the back of an Olympus BX61WI microscope. An Olympus LUMPlanFL 20×, 0.95 NA water immersion objective lens was used to focus the excitation light and collect the emission light. NIR laser excitation light and visible emission light were separated using a 750SP–2P AR–coated dichroic mirror (Chroma Technology). A 690/90 bandpass filter (Chroma Technology) and a focusing lens were used in front of the GaAs H7421–50 photomultiplier tube (Hamamatsu) to collect phosphorescent emission. Photon counting was performed using a SR430 multichannel scaler (Stanford Research Systems) to histogram the counts in 1024 or 2048 bins of 40 ns for aerated samples or 2.56 or 5.12 μs for FPT samples.

Energy transfer analysis

The efficiency of energy transfer (E) from the QD to the porphyrin was evaluated using Förster analysis,[32,53]

$$E = \frac{mk_{D-A}}{mk_{D-A} + \tau_D^{-1}} = \frac{mR_0^6}{mR_0^6 + r^6} \quad (2)$$

where k_{D-A} is the rate of energy transfer, r is the distance between the donor and acceptor, R_0 is the Förster distance or the distance at which the energy transfer efficiency is 50%, and m is the number of acceptor molecules per donor. This quantity can be measured experimentally:

$$E = 1 - \frac{\tau_{D-A}}{\tau_D} \quad (3)$$

where τ_D is the lifetime of the QD alone and τ_{D-A} is the lifetime of the QD with surface–bound porphyrin (**QD1–QD3**). Although the efficiency can be experimentally determined from the excited–state lifetime quenching, additional information is needed to quantify the parameters R_0, r, and m. The Förster distance is calculated using the following equation:

$$R_0^6 = \frac{9000(\ln 10)\kappa^2 \Phi_D}{128\pi^5 N n^4} \int_0^\infty F_D(\lambda)\varepsilon_A(\lambda)\lambda^4 d\lambda \quad (4)$$

where κ^2 is the relative orientation factor of the dipoles, taken to be 0.476 for static donor–acceptor orientations,[32,54] Φ_D is the quantum efficiency of the donor, N is Avogadro's number, and n is the index of refraction of the medium, which is taken to be 1.4961 for toluene.[55] The latter half of the equation represents the spectral overlap integral, often represented as J, where $F_D(\lambda)$ is the normalized intensity of the donor and $\varepsilon_A(\lambda)$ is the extinction coefficient of the acceptor at wavelength λ. Thus, R_0 may be calculated from the experimentally determined emission spectrum of the donor and the absorption spectrum of the acceptor.

X-ray crystallographic details

Diffraction quality crystals of **3** were obtained via slow vapor diffusion of heptane into a toluene solution of the compound, affording the crystals as orange blocks. Low–temperature (100 K) x–ray diffraction data was collected on a Siemens Platform three–circle diffractometer coupled to a Bruker– AXS Smart Apex CCD detector with graphite–monochromated Mo Kα radiation (λ, = 0.71073 Å), performing φ– and ω–scans. The data were processed and refined using the program SAINT supplied by Siemens Industrial Automation. The structure was solved by direct methods using SHELXS and refined against by standard difference Fourier techniques in the SHELXL program suite.[56] All hydrogen atoms were included in the model at geometrically calculated positions using a riding model and refined isotropically; all non–hydrogen atoms were refined anisotropically. Unit cell parameters, morphology, and solution statistics for the structure are summarized in Table S1. Thermal ellipsoid plots are drawn at the 50% probability level with hydrogen atoms omitted for clarity.

RESULTS AND DISCUSSION

Porphyrin Synthesis

The methodology to synthesize the free– base pyridyl porphyrins **1-H₂–3-H₂** was optimized by comparing the merits of various synthetic protocols for **1-H₂**. Initially, a mixed aldehyde

condensation under standard Lindsey conditions[57] was attempted, as this synthesis is well–known and works for a wide variety of *meso*–substituted porphyrins. However, only an insoluble black material was obtained in the attempted synthesis of **1-H$_2$**, likely due to the formation of polypyrrolic species. To circumvent these side reactions, a mixed aldehyde/dipyrromethane condensation[58] of 5–(4–pyridyl)dipyrromethane (**12**), 4–pyridinecarboxaldehyde, and methyl 4–formylbenzoate was performed under Lindsey conditions; no macrocyclic products were identified from this reaction. The failure of these reactions is presumably due to coordination of BF$_3$•OEt$_2$ to a pyridyl nitrogen, thereby sequestering the Lewis acid catalyst. While compound **1-H$_2$** has been prepared using Adler–Longo[59,60] porphyrin synthesis (Scheme S1),[61–64] this protocol suffers from difficult and repetitive chromatographic separations as all six possible porphyrin isomers (A$_4$, A$_3$B, *cis*–A$_2$B$_2$, *trans*–A$_2$B$_2$, AB$_3$, and B$_4$) are formed in addition to other tetrapyrrolic products, thus resulting in a low yield (4.3– 5.9%)[61–64] of the desired A3B product. Indeed, we could only obtain **1-H$_2$** under Adler–Longo conditions at 3.9% yield (see SI). An alternative to statistical methods is rational porphyrin synthetic methods, which involve the construction of a linear tetrapyrrole (i.e. bilane) that is cyclized and subsequently oxidized to afford the corresponding porphyrin.[65,66] This method has the advantage of forming a single porphyrin product, thereby circumventing difficult chromatographic separations. It also allows for the synthesis of porphyrin isomers that are difficult to isolate under statistical conditions (e.g., *cis*–A$_2$B$_2$ versus *trans*–A$_2$B$_2$). Additionally, up to four different *meso* substituents can be incorporated, thus enabling the formation of precise porphyrin isomers that are inaccessible with statistical methods (e.g., *cis*–A$_2$BC and ABCD). However, the rational synthesis (Scheme S2) of **1-H$_2$** entails a series of nine synthetic steps, with a yield of 15% (based on bilane precursor) for the combined bilane synthesis and subsequent porphyrin–forming steps.

A more facile synthesis of **1–3** is outlined in Figure 2. The method relies on the use of bilane precursors (1–acyl dipyrromethanes) in a MgBr$_2$–catalyzed [2+2] cycloaddition under microwave irradiation.[40] While, this is a statistical method of synthesis for **1**, the formation of only three porphyrin isomers (*trans*–A$_2$B$_2$, A$_3$B, and A$_4$) is possible. Using this method, porphyrin **1-H$_2$** was isolated in 11% yield. This nominal decrease in yield relative to the aforementioned bilane route is more than compensated by the elimination of three synthetic steps. This route is particularly amenable to the synthesis of *cis*–A$_2$B$_2$ porphyrins such as **2-H$_2$** for which the separation of the three porphyrins is facile. Similarly, **3-H$_2$** was synthesized in a [2+2] cycloaddition of a 1,9–diacyldipyrromethane and a dipyrromethane. By replacing the typical TFA acid catalyst[38] with Yb(OTf)$_3$, the yield of **3-H$_2$** was increased dramatically from 3.9% to 24%. In this case, the formation of only one porphyrin isomer is possible. Given the simplicity of this route and its advantages over both completely statistical and rational methods, the [2+2] route was preferred in the synthesis of **1-H$_2$–3-H$_2$**.

Palladium was introduced into the porphyrin macrocycle by using Pd(acac)$_2$ in pyridine under microwave irradiation.[67] This dramatically reduces the reaction time from as long as 4 d under conventional heating[68] to 20 min with microwave irradiation. Although the metallation reaction using this method is typically quantitative,[67] the observed yields here are low (17–50%). This is attributed to the formation of insoluble coordination oligomers in which Pd^{2+} coordinates to pyridyl groups of two different porphyrins, as has previously been observed.[69–72]

Diffraction quality crystals of **3** were obtained as orange blocks by slow vapor diffusion of heptane into a toluene solution of the compound. The thermal ellipsoid plot of the refined structure is shown in Figure 3 and a summary of the crystallographic data is of presented in Table S1. In order to identify the unique 4–pyridyl group of the structure, the 4 position of each *meso* substituent was refined as a carbon atom and the resultant electronic density

difference map was examined. The ten largest residual density peaks (Q peaks) of this refinement cycle are shown in Figure S1. Three of the four *meso* substituents show a Q peak adjacent to the 4 position of the ring, indicating the presence of a hydrogen atom, while the fourth does not, thereby differentiating the 4–pyridyl ring from the phenyl rings. Qualitatively, the structure is very similar to other Pd porphyrin complexes, such as 5,10,15,20–tetrakis(4– carboxy-phenyl)porphyrinatopalladium (II).[73] The palladium atom resides in the center of the 24 atom macrocycle plane with an average Pd–N distance of 2.011 Å (as compared to 2.009 Å for 5,10,15,20–tetraphenylporphyrinatopalladium(II), PdTPP).[74] The porphyrin plane exhibits an S_4 ruffle with an average deviation of 0.196 Å from the mean 24 atom plane. Such nonplanarity is also observed in the solid state structure of PdTPP. Each of the pyrrole nitrogen atoms deviates from the mean N_4 plane by 0.030 Å, a displacement that is identical to that observed for PdTPP.[74]

Electronic properties of porphyrins

Porphyrins **1–3** display absorption spectra (Figure 4) that are typical of hypsoporphyrins.[75,76] Table 1 summarizes the spectroscopic data for these porphyrins. The B band (Soret), centered at 415 nm, is intense and flanked by the weaker Q(1,0) and Q(0,0) bands at 523 and 554 nm, respectively. This absorption profile is similar to other *meso*– substituted Pd porphyrins. For comparison, PdTPP exhibits analogous absorbance features at 416, 522 and 551 nm.[77] The porphyrin emission spectra (Figure 4) (λ_{exc} = 525 nm) exhibits two broad emission bands with maxima observed at 690 nm for T(0,0) and 760 nm for T(0,1); these spectral features are similar to those observed for PdTPP (688 and ~760 nm).[77] Each porphyrin also exhibits a small emission feature ca. 606 nm that is attributed to the Q(0,1) fluorescence transition. This assignment is consistent with the insensitivity of the intensity of this band to oxygen; such a transition has been observed at 606 nm for PdTPP.[78]

The additional feature observed in the emission spectrum of **2** centered at 650 nm is assigned to the Q(0,0) transition of **2-H$_2$**. Based on the size of the emission band and the ten–fold higher emission quantum yield for H$_2$TTP (ϕ_f = 0.13)[79] as compared to that of the Pd complex (ϕ_p = 0.011 for **2**), it is estimated that **2-H$_2$** is present at most as a 1% impurity. In accordance with this contention, no trace *of* **2-H$_2$** was visible by NMR or TLC. Since the **2-H$_2$** fluorescence band is eclipsed by the phosphorescence bands of **2** in the absence of oxygen (Figure 4b) and the fluorescence lifetime of **2-H$_2$** (τ_{air} ~ 9 ns for free–base pyridyl porphyrins)[80] is much shorter than **2** (τ_{air} ~ 300 ns), the trace presence of this species has little impact on the results presented herein.

The phosphorescence quantum yields of **1–3** are between 1–2% and are comparable to other Pd porphyrins (ϕ_p = 0.02 for PdTPP).[81] As shown in Figure 4, the phosphorescence is quenched significantly by air, establishing that these compounds are responsive to oxygen in the 0–160 torr range. Indeed, the phosphorescence emission intensity from a freeze–pumped thawed (FPT) sample of **1** is 500–fold that observed for the sample in air; a 100–fold to 200–fold enhancement was observed for **2** and **3**.

The triplet lifetime (λ_{exc} = 525 nm) data of **1–3** in toluene at room temperature in the presence and absence of air is summarized in Table 2. Decay traces were fit at t > 100 ns to a monoexponential decay curve (R_{adj}^2 > 0.96). The significant difference in the lifetimes of **1–3** in the presence (~300 ns) and absence of air (~150 μs) suggests that these phosphors have a sufficient dynamic range to accurately quantify oxygen over a 0–160 torr range. Although porphyrins have low two–photon cross sections, sufficient signal was acquired to measure the lifetimes of **1–3** under two–photon (λ_{exc} = 850 nm) excitation (Table 2). To the best of our knowledge, this is the first study that compares porphyrin lifetimes under one– and two–photon excitation. Due to differences in selection rules for one– and two–photon

transitions, different states are accessed with different vibronic coupling.[82] It has been shown for linear polyenes that these differences lead to different one– and two–photon lifetimes.[83] Accordingly, the differences in lifetimes of **1–3** under one– and two–excitation are not unexpected.

QD Quenching Titrations with 1–3

Titration experiments were performed to assess surface binding of pyridyl porphyrins **1–3** to the surface of QD. In these titrations, there exists the following equilibrium,

$$QD + Por \underset{K_D}{\overset{K_A}{\rightleftharpoons}} QD - Por \quad (5)$$
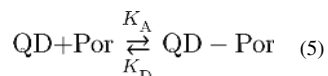
with an equilibrium constant K_A. Upon increasing the amount of porphyrin, the equilibrium is driven to conjugate formation. The QD emission provides a convenient probe of the equilibrium. For these experiments, the QD was judiciously chosen such that its emission overlapped with the absorbance of Q(1,0) of **1–3**, thereby maximizing the spectral overlap integral J (Eq. 4) and accordingly enabling quenching of QD emission by energy transfer. Specifically, we selected a QD with a first absorbance feature at 501 nm and emission band (λ_{exc} = 450 nm) centered at 519 nm (Figure S2).

The quenching of QD luminescence via energy transfer was examined as a function of the disposition of pyridyl rings at the *meso* positions: two *cis* 4–pyridyl rings (**1**), two *cis* 3–pyridyl rings (**2**), and a single 4–pyridyl ring (**3**). Titrations were performed in which the same amount of QD (~400 picomoles or ~100 nM) was treated with 1, 2, 5 or 10 equivalents of **1–3**. Each sample point in the titration was prepared independently and incubated overnight at room temperature to ensure porphyrin binding on the QD surface. Figure 5 shows the absorption, steady–state emission and time–resolved emission profiles for the titration of QD with **1**; similar data for compounds **2** and **3** are presented in Figures S3 and S4, respectively. The excitation wavelength of 450 nm was chosen for these experiments because the absorbance of the porphyrin is minimal whereas that of the QD is relatively high.

The absorption profile (Figure 5a) is effectively the sum of the QD and compound profiles. Figures 5b and 5c establish significant quenching of the QD emission with increasing concentration of the porphyrin. The quenching lifetimes obtained from the decay profiles in Figure 5c are provided in Table S2. We note that the emission decay of QD in the absence of porphyrin is biexponential (R_{adj}^2 > 0.99) with components that reflect surface trapped states (17 ns) and exciton emission (5 ns).[84,85] While QD lifetimes have been fit to triexponential functions[86,87] to include Auger recombination,[88] the inclusion of a third term is an overparameterization of our data. Biexponential behavior is preserved upon titration with porphyrin. Of the three compounds, **2**, with its *cis* disposition of pyridyl rings, quenches QD emission most effectively whereas **3**, with its single pyridyl ring is the least effective quencher. These results clearly suggest that two *cis* pyridyl rings facilitate porphyrin binding to the QD surface.

Since the formation of the QD/porphyrin conjugate occurs under dynamic self–assembly, there exists a discrete distribution of the number of porphyrins attached to the QD; hence there is a distribution of QD:porphyrin ratios at any point in the titration. Such a distribution is best described with Poisson statistics.[80] The Poisson probability distribution provides a model for the probability, $p(Y)$, that the number of events Y (i.e., a given QD:porphyrin ratio) occur, where λ is the average value of Y[89]

$$p(Y) = \frac{\lambda^Y}{Y!} e^{-\lambda} \quad (6)$$

where $Y = 0, 1, 2, \ldots,$ and $\lambda > 0$. For example, after the addition of one equivalent of porphyrin per equivalent of QD ($\lambda = 1$), the probability $p(Y)$ that there are 0, 1, 2, or ≥ 3 porphyrins per QD is 0.368, 0.368, 0.184, and 0.080, respectively.

As with the QD alone, the presence of porphyrin gives rise to a biexponential decay. Both the exciton emission (short lifetime component) and surface trapped state (long lifetime component) are affected by the presence of porphyrin. Because the surface state is most perturbed by porphyrin binding, the amplitude of the long lifetime component was used as a metric for determining the amount of free QD in solution. To this end, the long component of each decay was fixed at 16.93 ns, which is the calculated lifetime of the surface–trapped states for the QD alone. The relative reduction in the amplitude of this component serves as a measure of free QD at various points in the titration. The lifetime data is summarized in Table S2. Over the course of the titration, the surface trapped state is quenched, resulting in the formation of a non–fluorescent QD– porphyrin complex (*i.e.* static quenching). Based on the data, ten equivalents of **1** and **2** reduce the QD lifetime to ~300 ps with a similar emission intensity (*vide supra*), indicating that the *cis* pyridyl groups enhance QD surface binding and result in efficient luminescence quenching.

For 1 equivalent of **1**, the long component (surface trapped states) is reduced to 12% of the overall fit (compared to 53% for free QD), suggesting that ~20% of the QDs in solution lack a surface bound porphyrin. If the distribution of species in solution were purely statistical (*i.e.* non–specific interactions or encounter complexes), one would expect that ~37% of QDs would lack a surface bound porphyrin based on the Poission distribution. Since we observe fewer free QDs in solution, it is clear that **1** is binding to the QD surface in a directed manner. This is more clearly illustrated with **2**, which shows virtually no free QDs in solution after the addition of 1 equivalent of porphyrin. The fact that these two compounds do not follow the expected Poission distribution indicates that the QD–porphyrin interaction is specific (i.e. directed bidentate surface binding) and not just a statistical non– specific interaction. These observations are in stark contrast to compound **3**. After the addition of 1 equivalent of **3**, the amplitude of the long component is reduced to 12%, suggestive of 47% free QDs in solution. This is consistent with the expected value of 37% based on the Poisson distribution. The binding of **3** is so inefficient that ~34% of QDs are free in solution after the addition of 2 equivalents (compare to an expected 13% based on the Poisson distribution). Since the titration with **3** matches the expected Poisson distribution, the interaction between this molecule and the QD is nonspecific, suggesting that the interaction is statistical rather than directed. These results are consistent with the proposal that **1** and **2** are immobilized via a two point attachment, while porphyrin **3**, with a single 4–pyridyl group, results in less efficient luminescence quenching.

Whereas the distribution of species at low porphyrin concentration can be probed using QD lifetime data as a measure of free QD in solution, the lack of a suitable spectroscopic signature at high porphyrin concentrations renders the experimental determination of QD–porphyrin ratios intractable. At low porphyrin concentrations, the distribution of species in solution is dictated by the porphyrin's affinity for the surface (i.e. equilibrium constants as described below). At high porphyrin concentrations, geometric and steric factors control the distribution of QD–porphyrin species. Therefore, it is expected that this phenomenon is stochastic and follows a Poisson distribution.[80]

Determination of Equilibrium Constants

Using both the QD emission intensity and lifetime titration data, the equilibrium constant (K_A) for the formation of the QD–porphyrin conjugate (Eq. 5) was determined. The association constant can be determined using the Stern–Volmer equation:

$$\frac{I_o}{I} = \frac{\tau_o}{\tau} = 1 + K_A [\text{Por}] \quad (7)$$

where I_o and τ_o are the emission intensity and lifetime, respectively, in the absence of added porphyrin, I and τ are the emission intensity and lifetime, respectively, in the presence of a given concentration of porphyrin, [Por]. For all three porphyrins, both the lifetime (short component of Table S2) and intensity data are consistent, giving qualitatively similar plots (Figure S5). Downward curvature in the plots of the stronger ligators **1** and **2** at high porphyrin concentrations suggests a binding saturation event while **3** exhibits a linear plot. The linear regions of the data (Table S3) were fit to Eq. 7 to give average values of $K_A = 2.50 \times 10^7$ M^{-1} (**1**), 2.83×10^7 M^{-1} (**2**) and 1.36×10^6 M^{-1} (**3**). These results are consistent with the data of Figures 5, S3 and S4, indicating that **1** and **2** bind to the QD surface with similar efficacy whereas **3** binds more weakly. At high porphyrin concentrations, the curvature of **1** and **2** may be modeled with the Hill equation, which accounts for binding cooperativity:

$$y = y_{max} \frac{[\text{Por}]^n}{K_D^n + [\text{Por}]^n} \quad (8)$$

where y_{max} is the theoretical maximum value of y (I_0/I or τ_0/τ) at infinite substrate concentration and is a measure of the maximum extent of quenching of lifetime or emission intensity. K_D is the dissociation constant ($K_D = 1/K_A$) and n is the Hill coefficient, which is a measure of the degree of binding cooperativity. Positive cooperativity, i.e. the binding of one molecule facilitates subsequent binding event, is indicated for $n > 1$. For $n < 1$, there is negative cooperativity such that the binding of one molecule impedes the binding of additional molecules. If $n = 1$, binding is not cooperative and each binding event is independent. The fits of the data for **1** and **2** to Eq. 8 are presented in Table S4. For both intensity and lifetime data, the calculated y_{max} is very close to the observed y values at 10 equivalents, suggesting that binding saturation to a QD is reached at a limiting value of 10 equivalents of **1** and **2**. The different values of $n = 1.8$ for **1** and $n = 0.8$ for **2**, may reflect the different coordination modes of the porphyrins on the QD surface. π–stacking of **1** between porphyrin rings could lead to a positive cooperativity through π–π stacking interactions that facilitate the binding of subsequent porphyrin molecules. Conversely, an angled conformation in which the porphyrin covers the surface of the QD, would inhibit the binding of neighboring porphyrin molecules. This binding model is supported by titration experiments in which one equivalent of **2** dramatically quenches QD (Figure S3 and Table S2); we suspect this is because of the proximity of the porphyrin macrocycle to the QD surface.

Characterization of QD–porphyrin conjugates

Given the results of the titration experiments, 10 equivalents of porphyrin drives the equilibrium in Eq. 5 far to the right and ensures that each QD is associated to porphyrin. From Eq. 6, the probability of having a free QD at 10 equivalents of porphyrin in solution is essentially 0 (0.0045%). Conjugates prepared from 10 equivalents of porphyrin are designated **QD1–QD3**.

Table 1 lists selected steady–state absorption and emission spectroscopic data for the self–assembled **QD1–QD3** conjugates. The absorption spectrum of the conjugates is a composite sum of the porphyrin and QD spectra, as illustrated in Figure 6 for **QD1**. The emission spectra (λ_{exc} = 450 nm) also exhibit features characteristic of both the porphyrin and QD. As shown in Figure 7, a slight 1–2 nm (~ 100 cm^{-1} for B bands and ~ 40 cm^{-1} for Q bands) red shift was observed in the porphyrin absorption and emission bands of **QD1–QD3** as compared to **1–3**. This phenomenon, which has been observed for free–base porphyrins[90] and pyrene[25] bound to a QD surface, has been attributed to differences between the average dielectric constant of the lumophore in solution as compared to that near the surface of the QD. The QD emission from the conjugate is slightly blue–shifted (1–3 nm, 40–100 cm^{-1}) relative to free QD, which has previously been ascribed to modulation of the QD surface states[91,92] upon ligand binding.[93] More pronounced than these slight wavelength shifts is the increase in porphyrin phosphorescence quantum yield when bound to the QD (Table 1); **QD1** and **QD2** show the greatest enhancement (nearly a three–fold increase) in quantum yield upon surface binding as compared to **QD3**. This phenomenon has been attributed to a decrease in k_{nr} when the porphyrin is intercalating within the capping ligand environment.[9] These observations are concordant with stronger association of **1** and **2** to the QD surface than as compared to **3** owing to the *cis*–disposition of pyridyl ligands at the *meso* sites of the porphyrin framework of the former. Because the intensity of the T(0,0) porphyrin and QD emissions of **QD1** and **QD2** are comparable, a self–referencing scheme is easily established with these conjugates. This is not the case of **QD3**, which displays weak porphyrin emission as compared to the QD emission. The O$_2$ response is reversible, as the phosphorescence intensity is recovered upon subjecting an aerated sample to a freeze–pump–thaw cycle. This process may be repeated with no change in intensity.

The enhancement of porphyrin emission upon association of the QD is a result of FRET. In these assemblies, the QD serves as the antenna for photon absorption. Energy is passed from the QD donor to the porphyrin acceptor by the FRET mechanism. Under linear excitation (λ_{exc} = 450 nm), a nearly four–fold enhancement in emission is observed when QD is present (Figure S6) owing to the greater absorbance of the QD at 450 nm relative to **1**.

The FRET parameters for **QD1–QD3** are summarized in Table S5 and the spectral overlap of QD donor and porphyrin acceptor is illustrated in Figure S7. *J* is similar for all three assemblies and thus Förster distances (R_0) for the QD–porphyrin conjugates are also similar. Nevertheless, the FRET efficiencies, as calculated from the short component of the QD lifetimes at 10 equivalents (Table S2) and Eq. 3, vary significantly owing to differences in the interaction of the porphyrin with QD. The efficiency is 94% for **1** and **2**, but only 67% for **3**. The disparate conjugate interactions are unveiled in the donor–acceptor distances calculated from Eq. 2. *r* is significantly (~1.5 nm) longer in **QD3** as compared to **QD1** and **QD2**. These data again indicate that the *cis* disposition of the *meso* pyridyl substituents results in a tighter and more compact QD:porphyrin conjugate. The similarity of *r* for **QD1** and **QD2** indicate that the substitution motif (4–pyridyl versus 3–pyridyl) is not crucial to the FRET efficiency.

The consequences of the FRET efficiency calculations are revealed in the excitation spectra of **QD1–QD3** in Figure 8, which were recorded by monitoring the porphyrin emission at 685 nm with a 5 nm bandwidth. All of the collected emission is attributed to the porphyrin, as QD emission is spectrally separated by over 150 nm. At wavelengths where the porphyrins do not readily absorb (< 375 nm), a substantial emission signal is observed. This cannot be attributed to porphyrin absorption and subsequent emission. Instead, the QD absorbs the incident photons and transfers energy to the porphyrin which then emits. These excitation spectra correspond to the absorption profile of the conjugates (Figure 6), reflecting both porphyrin and QD absorption profiles. If the QD were not acting as a FRET

donor, the excitation spectra would look like the absorption profiles of **1–3**. Because of the similar extinction coefficients of **1–3**, the excitation spectra of these compounds should be the same in the absence of other effects. However, this is not the case because the FRET is modulated by the association of porphyrin to the QD. Accordingly, concentration–matched solutions of **QD1–QD3** show that **QD3** produces the least emission signal (since **3** is the weakest binder), having an intensity that is approximately 50% of **QD1**.

The FRET enhancement of porphyrin emission via the QD donor is more dramatic under two–photon excitation (λ_{exc} = 800 nm), as the two–photon absorption cross–section for QD is ~10^4 times greater than for the porphyrin itself. Figure 9 shows the two–photon emission spectrum for concentration–matched solutions of QD, **1**, and **QD1**. The porphyrin emission in **QD1** relative to **1** is enhanced by 10–fold and at the same time, the QD emission is reduced by ~70% in **QD1** relative to QD. These results indicate that the QD serves as a photon antenna and FRET donor, resulting in enhanced porphyrin emission under both one– and two–photon excitation.

Although **QD1–QD3** show a qualitatively similar response to oxygen as do **1–3**, evidenced by the difference in the emission intensity (Figure 7) in the presence and absence of air, the relative extent of quenching is not as great as the free porphyrin in solution. This observation is attributed to the overall lower amount of signal due to the FRET excitation of the porphyrin in **QD1–QD3** relative to direct excitation of Q(1,0) in **1–3**. Air quenches the T(0,0)emission of **QD1** by 100 and by 50 fold for T(0,1). **QD2** is somewhat less sensitive with approximately a 50–fold effect for both transitions whereas only a 10–fold effect is observed for **QD3**, presumably due to the lower FRET efficiency and thus lower amount of total signal.

Triplet lifetimes (λ_{exc} = 450 nm) of **QD1–QD3** were determined in toluene at room temperature under both air and for FPT solutions (Table 3). Decay traces at t >100 ns were fit to a biexponential decay curve (R_{adj}^2 > 0.96). With an increase in quantum yield of the porphyrin within the QD construct, a similar increase in lifetime is expected based on

$$\Phi = \frac{k_r}{k_r + k_{nr}} = k_r \tau_c \quad (9)$$

As expected, the long component of the decay is significantly longer than free porphyrin by over 300 ns for air measurements and 550 μs for FPT measurements (see Table 2). Such observations have been previously reported for other fluorophore systems.[9,25,85] The significantly longer component is attributed to the intercalation of the porphyrin into the passivating ligand that coats the QD surface; this protects the porphyrin from molecular collisions and other nonradiative decay processes, thereby extending the radiative lifetime. The shorter component is likely to be free porphyrin as this lifetime is comparable to free porphyrin in solution (~150 μs, Table 2). In air, the average lifetimes for the QD–porphyrin assemblies are significantly shortened, reflecting the quenching process observed by steady-state emission.

In addition to the one–photon lifetimes, the lifetimes of FPT and aerated samples of **QD1–QD3** were measured under two–photon irradiation (λ_{exc} = 850 nm) (Table 3). The observed lifetimes for **QD1** and **QD2** are consistent with the results of one–photon excitation. The FPT samples exhibit long (~200 μs) and short lifetime components (~50 μs, compared to ~150 μs for free porphyrin). The lifetimes of the conjugates in air under two–photon excitation reflect quenching, but the short lifetime, akin to what was observed in the one–photon case, is not resolved from the instrument response function.

CONCLUSIONS

Self–assembled QD–porphyrin nanosensor conjugates detect O_2 in the 0–160 torr range under both one– and two–photon excitation. Two *cis* pyridyl groups in the *meso* position of the Pd porphyrin macrocycle promote the most effective binding of the palladium porphyrin to the surface of a QD. The QD serves as one–or two–photon light harvesting antennae of the Pd porphyrin. Owing to the insensitivity of the QD to O_2, a ratiometric signal transduction mechanism may be established. Because of superior spectral overlap and efficient surface binding, the FRET efficiency in these systems is 67–94%.

The QD is essential in implementing sensing under two–photon conditions owing to the QD's high two–photon absorption cross–section (σ_2). Although free–base QD–porphyrin assemblies have been previously studied as FRET systems,[80,86,90] they have not been examined under two–photon excitation nor have been explored as sensors. Both ruthenium bipyridine complexes[94] and Pt porphyrins[95,96] have been used as O_2 sensors in conjunction with QDs, but in these systems the QD has served only as an internal intensity standard. Indeed the few examples of authentic FRET–based O_2 sensing include pyrene,[25] platinum octaethylporphyrin ketone,[97,98] or osmium bipyridine complexes[9] as the FRET acceptor. Of these, two–photon excitation of the FRET acceptor by QD has been achieved only with the osmium bipyridine complex. This system, however, suffers from low dynamic range at biologically relevant oxygen pressures (0–160 torr).[9] We now establish a viable two–photon O_2 sensing mechanism over this pressure range with **QD1–QD3**. Having fully characterized this system in organic solvents, we are currently developing methods to translate this system to water so that it can be used for *in vivo* two– photon oxygen sensing applications.

Supplementary Material

Refer to Web version on PubMed Central for supplementary material.

Acknowledgments

REFERENCES

1. Vaupel P, Kallinowski F, Okunieff P. Cancer Res. 1989; 49:6449–6465. [PubMed: 2684393]

2. Helmlinger G, Yuan F, Dellian M, Jain RK. Nat. Med. 1997; 3:177–182. [PubMed: 9018236]

3. Chauhan VP, Stylianopoulos T, Boucher Y, Jain RK. Annu. Rev. Chem. Biomol. Eng. 2011; 2:281–298. [PubMed: 22432620]

4. Folkman J. Nat. Rev. Drug Discovery. 2007; 6:273–286.

5. Jain RK. Science. 2005; 307:58–62. [PubMed: 15637262]

6. Snee PT, Somers RC, Nair G, Zimmer JP, Bawendi MG, Nocera DG. J. Am. Chem. Soc. 2006; 128:13320–13321. [PubMed: 17031920]

7. Somers RC, Lanning RM, Snee PT, Greytak AB, Jain RK, Bawendi MG, Nocera DG. Chem. Sci. 2012; 3:2980–2985.

8. Kay ER, Lee J, Nocera DG, Bawendi MG. Angew. Chem. Int .Ed. 2013; 52:1165–1169.

9. McLaurin EJ, Greytak AB, Bawendi MG, Nocera DG. J. Am. Chem. Soc. 2009; 131:12994–13001. [PubMed: 19697933]

10. Murray CB, Norris DJ, Bawendi MG. J. Am. Chem. Soc. 1993; 115:8706–8715.

11. Alivisatos P. Nat. Biotechnol. 2004; 22:47–52. [PubMed: 14704706]

12. Xia Z, Rao J. Curr. Opin. Biotechnol. 2009; 20:37–44. [PubMed: 19216068]

13. Baltazar, R.; Vistas, CR.; Ferreira, GNM. Nanocomposite Particles for Bio-Applications: Materials and Bio-Interfaces. Trindade, T.; Silva da, ALD., editors. Boca Raton, FL: Taylor & Francis; 2012. p. 265-282.

14. Medintz IL, Clapp AR, Mattoussi H, Goldman ER, Fisher B, Mauro JM. Nat. Mater. 2003; 2:630–638. [PubMed: 12942071]

15. Somers RC, Bawendi MG, Nocera DG. Chem. Soc. Rev. 2007; 36:579–591. [PubMed: 17387407]

16. Suzuki M, Husimi Y, Komatsu H, Suzuki K, Douglas KT. J. Am. Chem. Soc. 2008; 130:5720–5725. [PubMed: 18393422]

17. Blanton SA, Dehestani A, Lin PC, Guyot-Sionnest P. Chem. Phys. Lett. 1994; 229:317–322.

18. Larson DR, Zipfel WR, Williams RM, Clark SW, Bruchez MP, Wise FW, Webb WW. Science. 2003; 300:434–1436.

19. Pu SC, Yang MJ, Hsu CC, Lai CW, Hsieh CC, Lin SH, Cheng YM, Chou PT. Small. 2006; 2:1308–1313. [PubMed: 17192978]

20. Richards-Kortum R, Sevick-Muraca E. Annu. Rev. Phys. Chem. 1996; 47:555–606. [PubMed: 8930102]

21. Zipfel WR, Williams RM, Webb WW. Nat. Biotechnol. 2003; 21:1369–1377. [PubMed: 14595365]

22. Jain, RK.; Booth, MF.; Padera, TP.; Munn, LL.; Fukumura, D.; Brown, E. Handbook of Biomedical Nonlinear Optical Microscopy. Masters, BR.; So, PTC., editors. New York: Oxford University Press; 2008. p. 735-756.

23. Yoshihara T, Yamaguchi Y, Hosaka M, Takeuchi T, Tobita S. Angew. Chem. Int. Ed. 2012; 51:4148–4151.

24. Coogan MP, Court JB, Gray VL, Hayes AJ, Lloyd AH, Millet CO, Pope SJA, Lloyd D. Photochem. Photobiol. Sci. 2010; 9:103–109. [PubMed: 20062850]

25. Amelia M, Lavie-Cambot A, McClenaghan ND, Credi A. Chem. Commun. 2011; 47:325–327.

26. Okura, I.; Kamachi, T. Handbook of Porphyrin Science. Kadish, KM.; Smith, KM.; Guilard, R., editors. Vol. Vol. 12. Singapore: World Scientific Publishing; 2011. p. 297-348.

27. Tripathi VS, Lakshminarayana G, Nogami M. Sens. Actuators B. 2010; 147:741–747.

28. Wang X, Meier RJ, Link M, Wolfbeis OS. Angew. Chem. Int. Ed. 2010; 49:4907–4909.

29. Amao Y, Miyakawa K, Okura I. J. Mater. Chem. 2000; 10:305–308.

30. Zhang H, Sun Y, Ye K, Zhang P, Wang Y. J. Mater. Chem. 2005; 15:3181–3186.

31. Dunphy I, Vinogradov SA, Wilson DF. Anal. Biochem. 2002; 310:191–198. [PubMed: 12423638]

32. Lakowicz, JR. Principles of Fluorescence Spectroscopy. 3rd ed. New York: Springer; 2006.

33. Kruk M, Karotki A, Drobizhev M, Kuzmitsky V, Gael V, Rebane A. J. Lumin. 2003; 105:45–55.

34. Briñas RP, Troxler T, Hochstrasser RM, Vinogradov SA. J. Am. Chem. Soc. 2005; 127:11851–11862. [PubMed: 16104764]

35. Finikova OS, Troxler T, Senes A, DeGrado WF, Hochstrasser RM, Vinogradov SA. J. Phys. Chem. A. 2007; 111:6977–6990. [PubMed: 17608457]

36. Finikova OS, Lebedev AY, Aprelev A, Troxler T, Gao F, Garnacho C, Muro S, Hochstrasser RM, Vinogradov SA. ChemPhysChem. 2008; 9:1673–1679. [PubMed: 18663708]

37. Sinks LE, Robbins GP, Roussakis E, Troxler T, Hammer DA, Vinogradov SA. J. Phys. Chem. B. 2010; 114:14373–14382. [PubMed: 20462225]

38. Gryko D, Lindsey JS. J. Org. Chem. 2000; 65:2249–2252. [PubMed: 10774058]

39. Zaidi SHH, Muthukumaran K, Tamaru S, Lindsey JS. J. Org. Chem. 2004; 69:8356–8365. [PubMed: 15549807]

40. Dogutan DK, Ptaszek M, Lindsey JS. J. Org. Chem. 2008; 73:6187–6201. [PubMed: 18637693]

41. Laha JK, Dhanalekshmi S, Taniguchi M, Ambroise A, Lindsey JS. Org. Process Res. Dev. 2003; 7:799–812.

42. Zaidi SHH, Loewe RS, Clark BA, Jacob MJ, Lindsey JS. Org. Process Res. Dev. 2006; 10:304–314.

43. Sharada DS, Muresan AZ, Muthukumaran K, Lindsey JS. J. Org. Chem. 2005; 70:3500–3510. [PubMed: 15844983]

44. Leatherdale CA, Woo WK, Mikulec FV, Bawendi MG. J. Phys. Chem. B. 2002; 106:7619–7622.

45. Fulmer GR, Miller AJM, Sherden NH, Gottlieb HE, Nudelman A, Stoltz BM, Bercaw JE, Goldberg KI. Organometallics. 2010; 29:2176–2179.

46. Suzuki K, Kobayashi A, Kaneko S, Takehira K, Yoshihara T, Ishida H, Shiina Y, Oishi S, Tobita S. Phys. Chem. Chem. Phys. 2009; 11:9850–9860. [PubMed: 19851565]

47. Grabolle M, Spieles M, Lesnyak V, Gaponik N, Eychmüller A, Resch-Genger U. Anal. Chem. 2008; 81:6285–6294.

48. Pizano AA, Lutterman DA, Holder PG, Teets TS, Stubbe J, Nocera DG. Proc. Natl. Acad. Sci. USA. 2012; 109:39–43. [PubMed: 22171005]

49. Holder PG, Pizano AA, Anderson BL, Stubbe J, Nocera DG. J. Am. Chem. Soc. 2012; 134:1172–1180. [PubMed: 22121977]

50. Loh ZH, Miller SE, Chang CJ, Carpenter SD, Nocera DG. J. Phys. Chem. A. 2002; 106:11700–11708.

51. Brown EB, Campbell RB, Tsuzuki Y, Xu L, Carmeliet P, Fukumura D, Jain RK. Nat. Med. 2001; 7:864–868. [PubMed: 11433354]

52. Lanning, RM. Ph.D. Thesis. Cambridge, MA, USA: Massachusetts Institute of Technology; 2009.

53. Förster T. Ann. Phys. 1948; 437:55–75.

54. Steinberg IZ. Annu. Rev. Biochem. 1971; 40:83–114. [PubMed: 4331120]

55. CRC Handbook of Chemistry and Physics. 84th ed. Boca Raton, FL: CRC Press; 2003.

56. Sheldrick GM. Acta Crystallogr., Sect. A: Found. Crystallogr. 2008; A64:112–122.

57. Lindsey JS, Wagner RW. J. Org. Chem. 1989; 54:828–836.

58. Lembo A, Tagliatesta P, Cicero D, Leoni A, Salvatori A. Org. Biomol. Chem. 2009; 7:1093–1096. [PubMed: 19262927]

59. Adler AD, Longo FR, Shergalis W. J. Am. Chem. Soc. 1964; 86:3145–3149.

60. Adler AD, Longo FR, Finarelli JD, Goldmacher J, Assour J, Korsakoff L. J. Org. Chem. 1967; 32:476.

61. Ishikawa Y, Yamashita A, Uni T. Chem. Pharm. Bull. 2001; 49:287–293. [PubMed: 11253918]

62. Sirish M, Chertkov VA, Schneider HJ. Chem. Eur. J. 2002; 8:1181–1188. [PubMed: 11891906]

63. Gianferrara T, Giust D, Bratsos I, Alessio E. Tetrahedron. 2007; 63:5506–5013.

64. Wu L, Hu P, Xiao Y, Zhang M, Zhang L, Weng X, Wu X, Zhou X, Cao X. Chem. Biodivers. 2008; 5:153–161. [PubMed: 18205117]

65. Dogutan DK, Zaidi SHH, Thamyongkit P, Lindsey JS. J. Org. Chem. 2007; 72:7701–7714. [PubMed: 17824652]

66. Dogutan DK, Lindsey JS. J. Org. Chem. 2008; 73:6728–6742. [PubMed: 18683982]

67. Dean M, Schmink JR, Leadbeater NE, Brückner C. Dalton Trans. 2008:1341–1345. [PubMed: 18305846]

68. Obata M, Matsuura N, Mitsuo K, Nagai H, Asai K, Harada M, Hirohara S, Tanihara M, Yano S. J. Polym. Sci. Part A: Polym. Chem. 2010; 48:663–670.

69. Milic TN, Chi N, Yablon DG, Flynn GW, Batteas JD, Drain CM. Angew. Chem. Int. Ed. 2002; 41:2117–2119.

70. Deiters E, Bulach V, Hosseini MW. New. J. Chem. 2006; 30:1289–1294.

71. Yedukondalu M, Ravikanth M. J. Chem. Sci. 2011; 123:201–214.

72. Li Y, Xiao J, Shubina TE, Chen M, Shi Z, Schmid M, Steinrück HP, Gottfried JM, Lin N. J. Am. Chem. Soc. 2012; 134:6401–6408. [PubMed: 22414052]

73. Lipstman S, Goldberg I. Acta Crystallogr. Sect. C: Cryst. Struct. Commun. 2008; C64:m53–m57.

74. Fleischer EB, Miller CK, Webb LE. J. Am. Chem. Soc. 1964; 86:2342–2347.

75. Gouterman, M. The Porphyrins. Dolphin, D., editor. Vol. Vol. 3. New York: Academic Press; 1978. p. 1-165.

76. Kalyanasundaram, K. Photochemistry of Polypyridine and Porphyrin Complexes. San Diego, CA: Academic Press; 1992. p. 498-502.

77. Eastwood D, Gouterman M. J. Mol. Spectrosc. 1970; 35:359–375.

78. Callis JB, Gouterman M, Jones YM, Henderson BH. J. Mol. Spectrosc. 1971; 39:410–420.

79. Quimby DJ, Longo FR. J. Am. Chem. Soc. 1975; 97:5111–5117.

80. Zenkevich EI, Sagun EI, Knyukshto VN, Stasheuski AS, Galievsky AV, Stupak AP, Blaudeck T, von Borczyskowsk C. J. Phys. Chem. C. 2011; 115:21535–21545.

81. Faure S, Stern C, Guilard R, Harvey PD. Inorg. Chem. 2005; 44:9232–9241. [PubMed: 16323904]

82. Bonin KD, McIlrath TJ. J. Opt. Soc. Am. B: Opt. Phys. 1984; 1:52–55.

83. Petek H, Bell AJ, Choi YS, Yoshihara K, Tounge BA, Christensen RL. J. Chem. Phys. 1995; 102:4726–4739.

84. Javier A, Magana D, Jennings T, Strouse GF. Appl. Phys. Lett. 2003; 83:1423–1425.

85. Wen Y, Liu Y, Yang Y, An L, Song W, Yang Z. J. Micro/Nanolith. MEMS MOEMS. 2010; 9:031003/1–031003/4.

86. Zenkevich EI, Sagun EI, Yarovoi AA, Shulga AM, Knyukshto VN, Stupak AP, von Borczyskowski C. Opt. Spectrosc. 2007; 103:958–968.

87. Jones M, Lo SS, Scholes GD. Proc. Natl. Acad. Sci. U.S.A. 2009; 106:3011–3016. [PubMed: 19218443]

88. Klimov VI, Mikhailovsky AA, Branch DW, Leatherdale CA, Bawendi MG. Science. 2000; 287:1011–1013. [PubMed: 10669406]

89. Wackerly, DD.; Mendenhall, W.; Scheaffer, RL. Mathematical Statistics with Applications. 6th ed. Pacific Grove, CA: Duxbury; 2002. p. 124-126.

90. Zenkevich E, Cichos F, Shulga A, Petrov EP, Blaudeck T, von Borczyskowski C. J. Phys. Chem. B. 2005; 109:8679–8692. [PubMed: 16852028]

91. Talapin DV, Rogach AL, Kornowski A, Hasse M, Weller H. Nano Lett. 2001; 1:207–211.

92. Balogh L, Zhang C, O'Brien S, Turro NJ, Brus L. Chim. Oggi. 2002; 20:45–51.

93. Bullen C, Mulvaney P. Langmuir. 2006; 22:3007–3013. [PubMed: 16548550]

94. Jorge PAS, Mayeh M, Benrashid R, Caldas P, Santos JL, Farahi F. Appl. Opt. 2006; 45:3760–3767. [PubMed: 16724134]

95. Collier BB, Singh S, McShane M. Analyst. 2011; 136:962–967. [PubMed: 21170467]

96. Wang X, Chen X, Xie Z, Wang X. Angew. Chem. Int. Ed. 2008; 47:7450–7453.

97. Zhang C, Ingram J, Schiff S, Xu J, Xiao M. Proc. SPIE. 2011; 7947:79470B-1–79470B-6.

98. Ingram JM, Zhang C, Xu J, Schiff SJ. J. Neurosci. Methods. 2013; 214:45–51. [PubMed: 23333398]
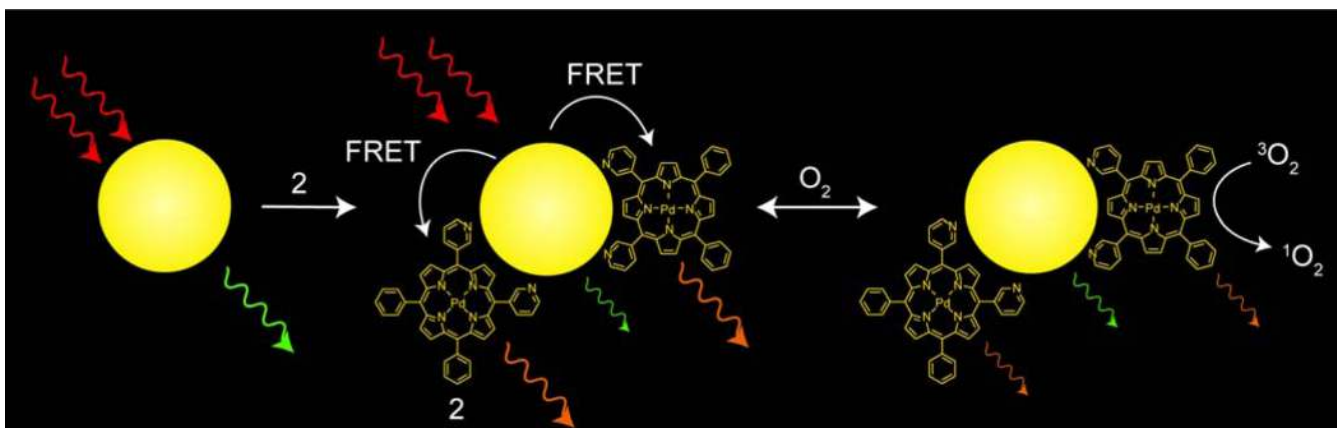
Figure 1.
Schematic representation of the O_2 sensing transduction mechanism of a self–assembled Pd porphyrin (**2**)–QD construct. The QD acts as the two–photon antenna of NIR (700–1000 nm) excitation. The QD emission is quenched in the presence of a surface–bound Pd porphyrin (**2**) via a FRET mechanism. The insensitivity of the QD emission to O_2 affords an internal reference to establish a ratiometric O_2 response.
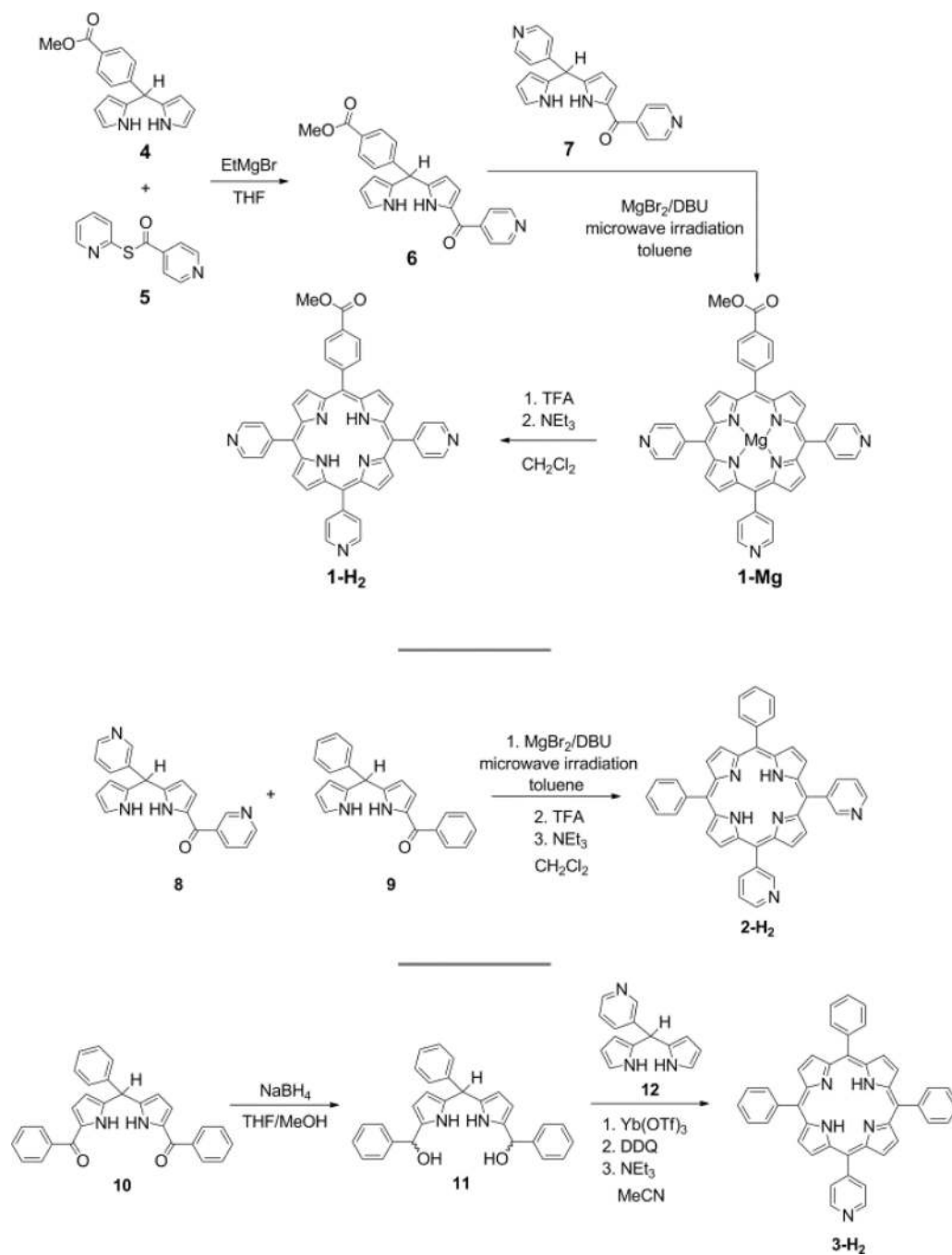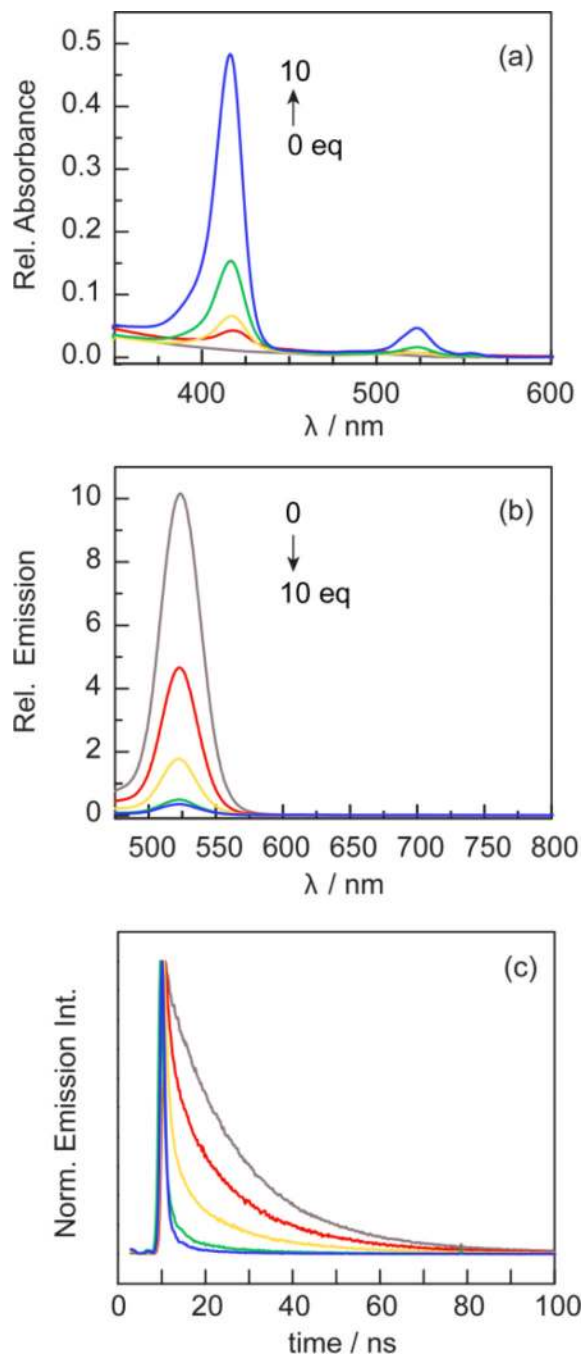
Figure 2.
Synthesis of **1–3** from metal–catalyzed [2+2] cycloadditions of appropriate bilane precursors.
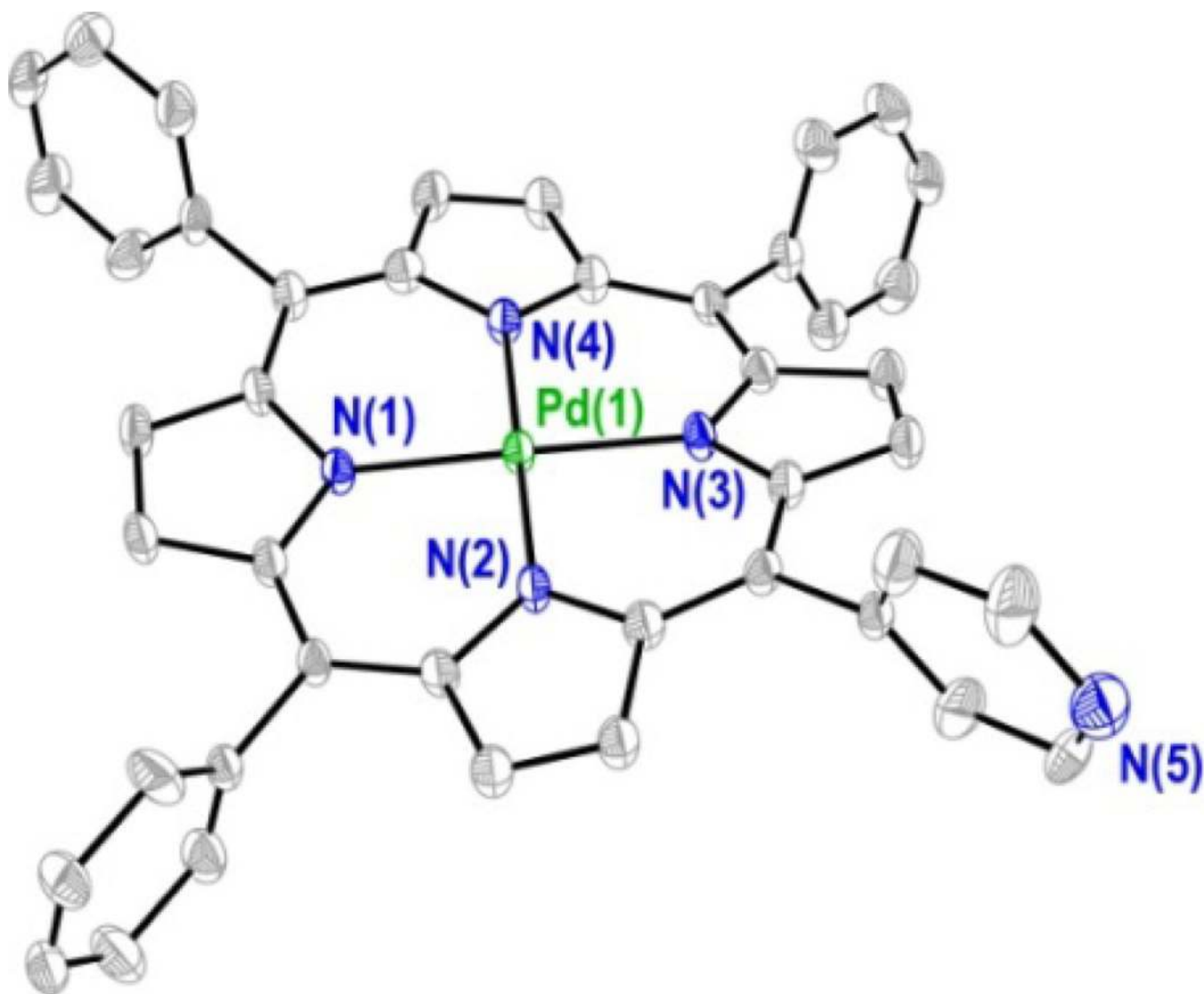
Figure 3.
Solid-state crystal structure of compound **3**. Thermal ellipsoids are drawn at the 50%
probability level and hydrogen atoms have been removed for clarity.
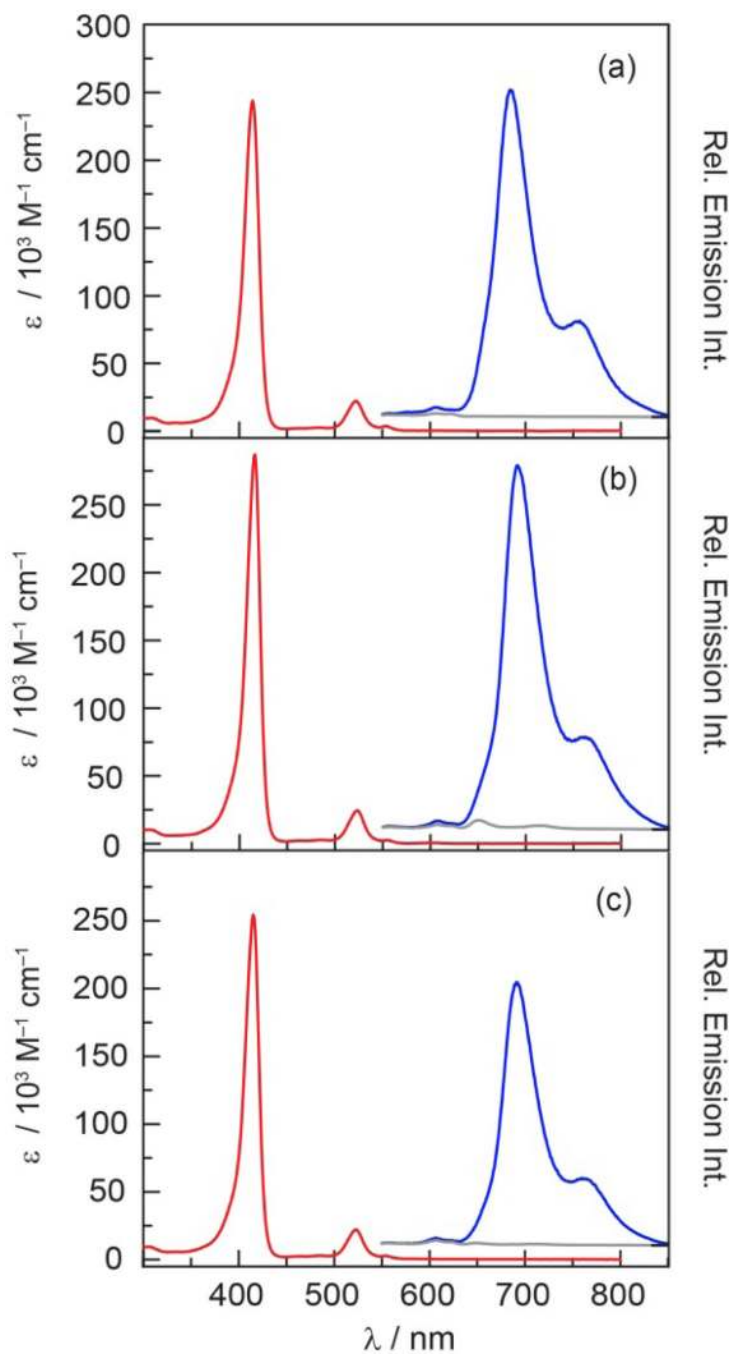
Figure 4.
Comparison of the steady state absorption (━) and emission spectra (λ_{exc} = 525 nm) of (a) **1,** (b) **2** and (c) **3** in the presence of air (~160 torr O_2) (━) and under vacuum (━) in toluene.

Figure 5.
Spectral changes associated with titration of a toluene solution of QD (—) with 1 (—), 2
(—), 5 (—) and 10 (—) equiv of **1**. Similar data for **2** and **3** are shown in Figures S3 and S4.
(a) The intensity of the Soret and Q band absorption profiles increases. (b) The QD emission
(λ_{exc} = 450 nm) intensity is quenched and (c) the decay profiles of the QD emission (λ_{exc} =
450 nm) decreases with increasing equivalents of **1**.
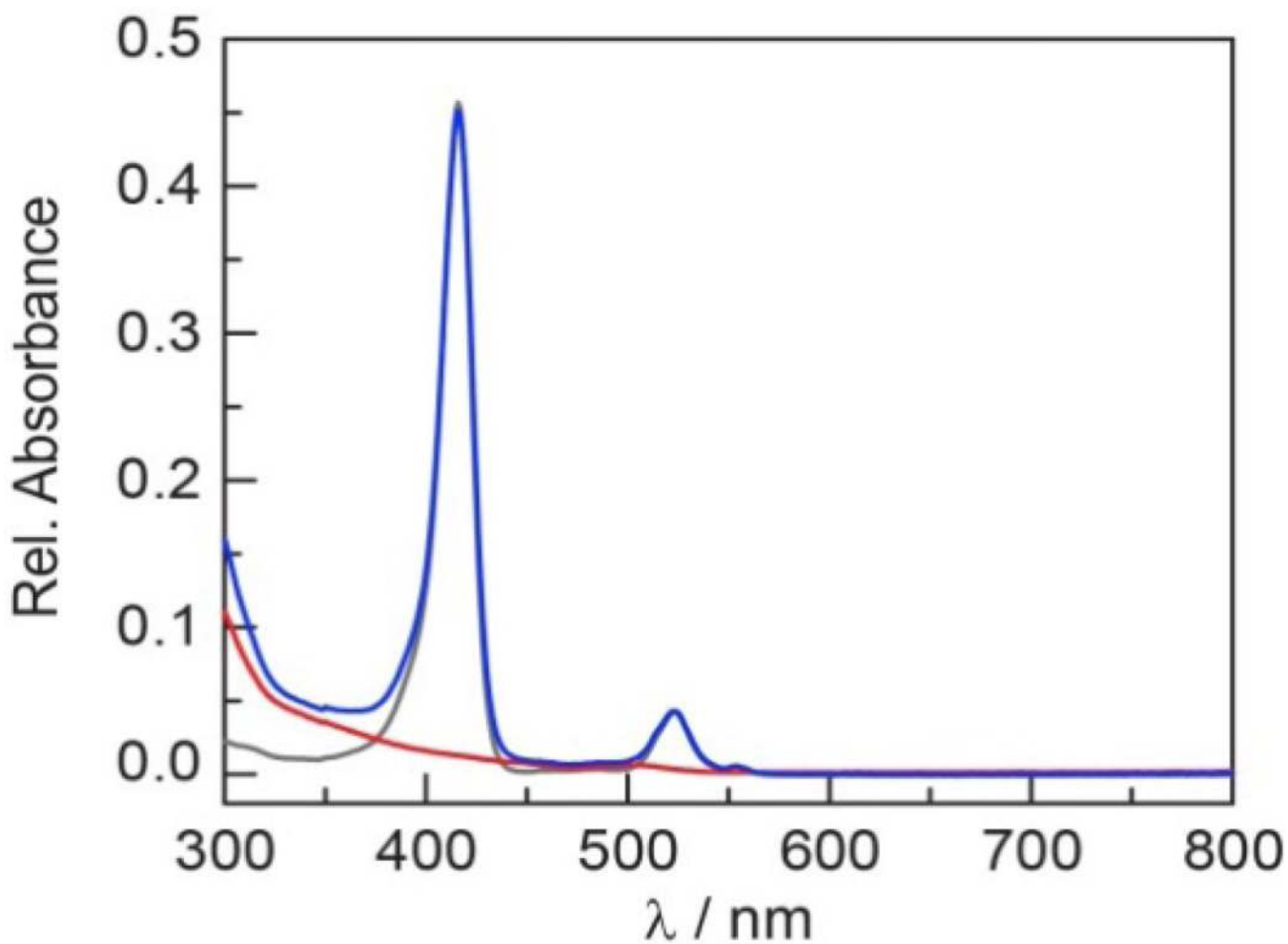
Figure 6.
Comparison of the absorption spectra of **1** (—), **QD** (—) and **QD1** (—) in toluene. The spectrum of **QD1** represents a composite of the two constituent spectra.
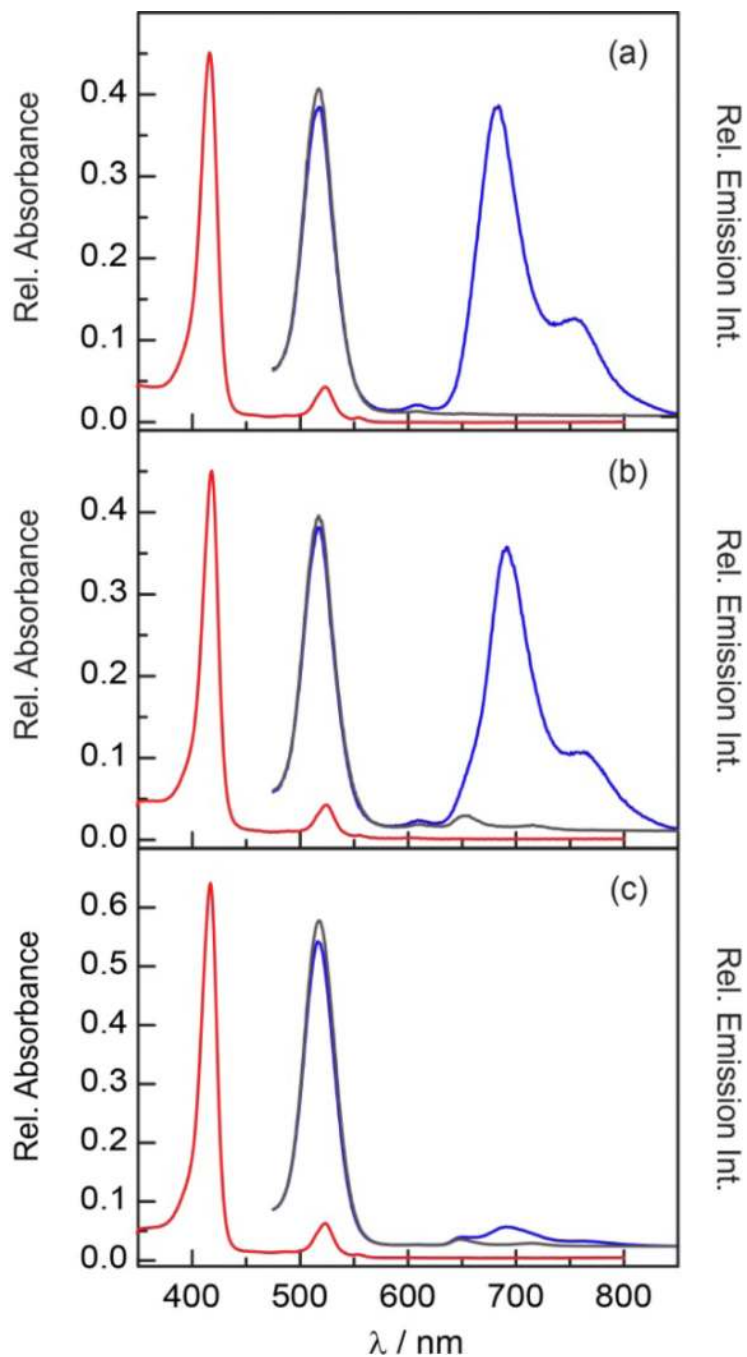
Figure 7.
Comparison of the steady state absorption (—) and emission spectra (λ_{exc} = 525 nm) of (a) **QD1**, (b) **QD2** and (c) **QD3** in the presence of air (~160 torr O_2) (—) and under vacuum (—) in toluene.
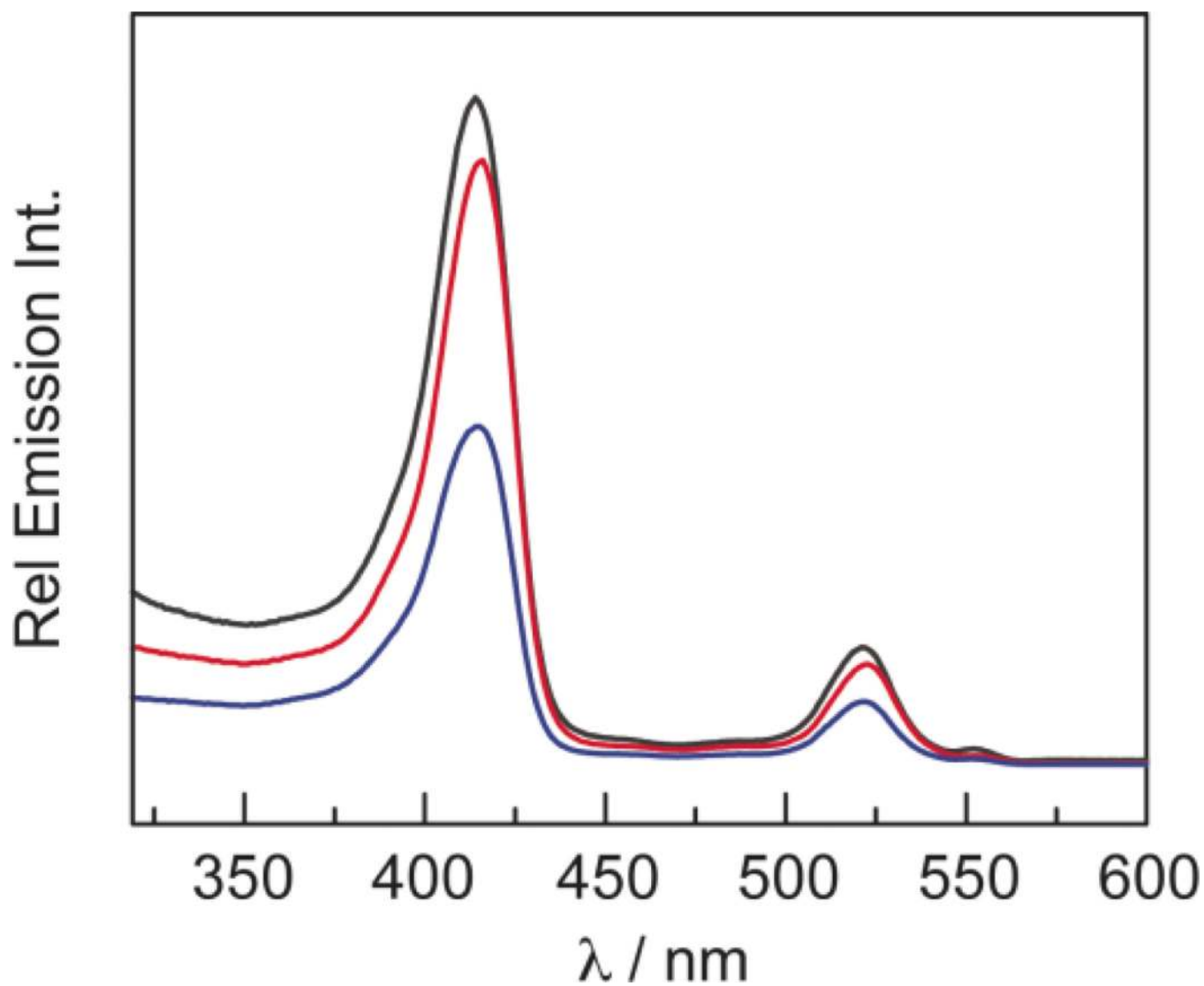
Figure 8.
Excitation spectra (λ_{em} = 685 nm) of concentration– matched toluene solutions of **QD1** (—),
QD2 (—) and **QD3** (—).
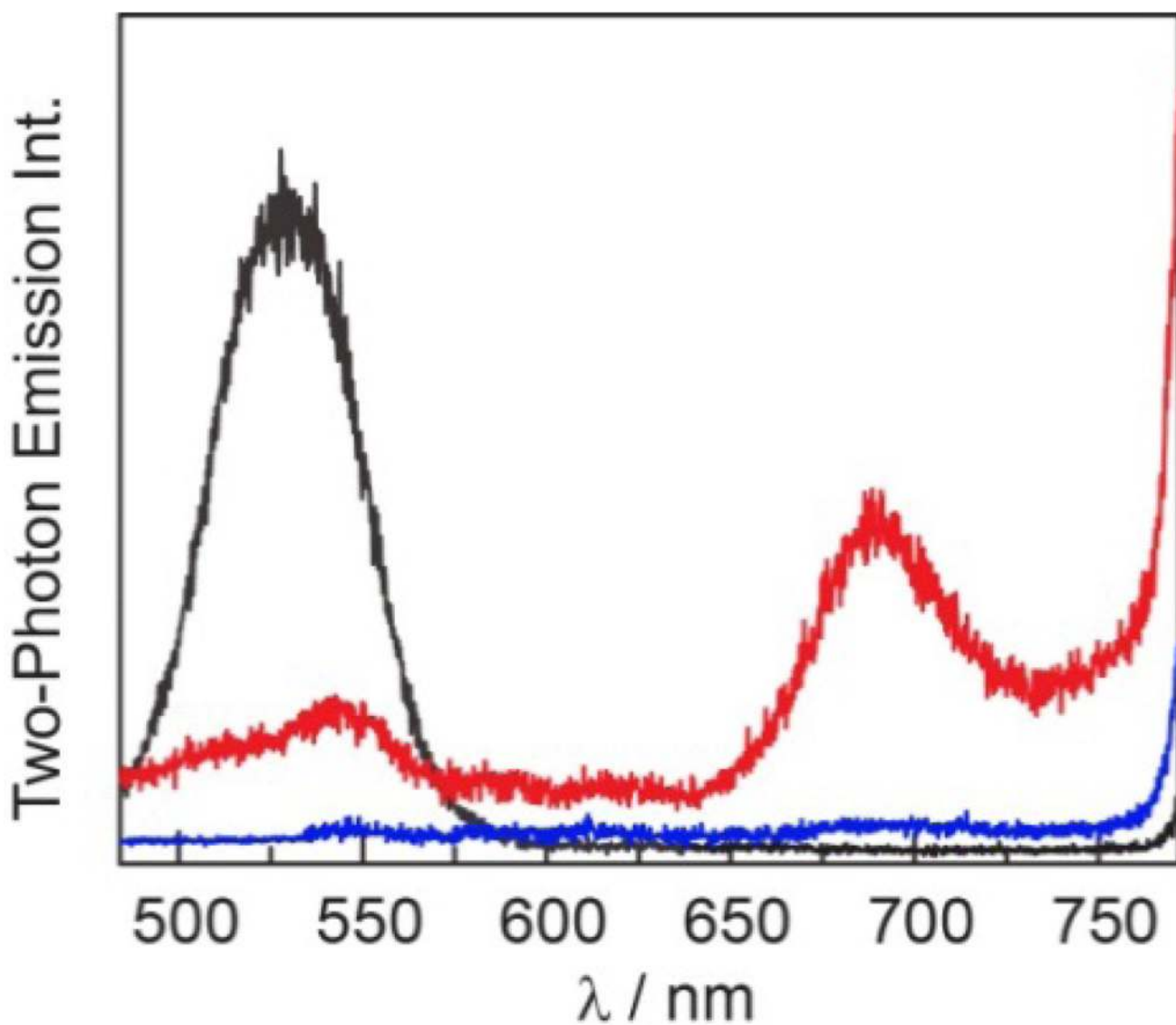
Figure 9.
Two–photon emission spectra *(λ*exc = 800 nm) of concentration–matched toluene solutions of QD (—) and freeze– pump–thawed solutions of **1** (—) and **QD1** (—). **1** does not emit under two–photon excitation and emission is only observable in the presence of QD.
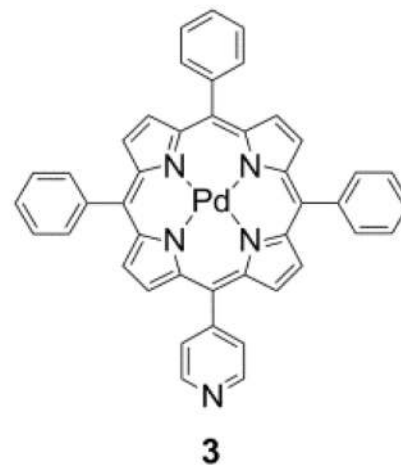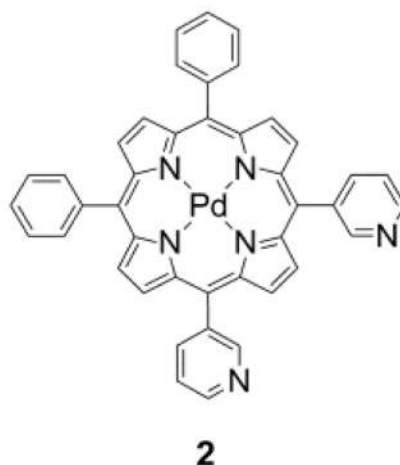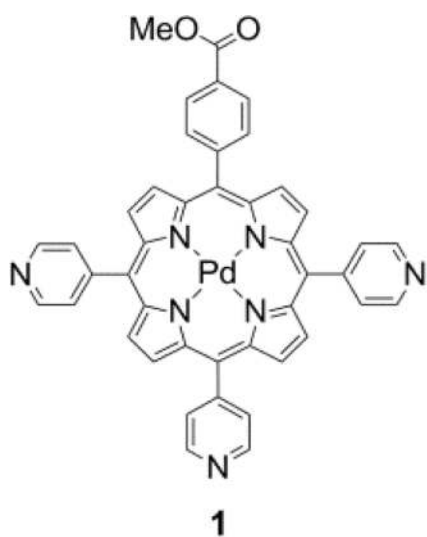
Chart 1.

Table 1

Summary of Linear Spectroscopic Data for Pd Porphyrins and QD Conjugates

Compound[a]	B(0,0), ε[b]	Q(1,0), ε[b]	Q(0,0), ε[b]	QD$_{Em}$	T(0,0)[c]	T(0,1)[c]	Φ_p[d]
1	414, 240	522, 22	554, 3.6	–	684	753	0.014
2	416, 290	523, 24	554, 2.6	–	691	760	0.011
3	415, 250	523, 22	554, 2.8	–	691	760	0.014
QD1	416	523	554	517	684	754	0.040
QD2	418	524	555	518	692	763	0.027
QD3	417	523	553	516	691	761	0.018

[a]Toluene solution, transition wavelengths are in units of nm.

[b]ε in 10^3 M^{-1} cm^{-1}, as determined in CH2Cl2.

[c]Triplet transitions for evacuated samples ($< 10^{-5}$ torr).

[d]Phosphorescence quantum yield of freeze–pump–thawed samples.

Table 2

Summary of Lifetime Data for Pd Porphyrins

Compound[a]	τ_{air} (ns) 1–photon[c]	τ_o (µs)[b] l-photon[c]	τ_{air} (ns) 2–photon[d]	τ_o (µs)[b] 2-photon[d]
1	332 ± 3[e]	154 ± 12	556 ± 40	157 ± 3
2	289 ± 7	133 ± 5	354 ± 14	77 ± 5
3	305 ± 6	144 ± 6	365 ± 12	80 ± 3

[a]Toluene solution.

[b]freeze–pump–thawed samples ($<10^{-5}$ torr).

[c]λ_{exc}= 525 nm.

[d]λ_{exc} = 850 nm.

[e]95% confidence interval.

Table 3

Summary of Porphyrin Triplet State Lifetime Data for Assemblies QD1–QD3

Compound[a]	Sample	λ_{exc}/nm	τ_1	A_1 (%)[b]	τ_2	A_2 (%)[b]	τ_{avg}[c]
QD1	air	450	638 ± 64 ns[d]	17	69 ± 11 ns	83	174 ± 92 ns
QD2	air	450	575 ± 5 ns	1	29 ± 1 ns	99	37 ± 1 ns
QD3	air	450	550 ± 6 ns	6	41 ± 1 ns	94	72 ± 7 ns
QD1	fpt[e]	450	590 ± 79 μs	75	149 ± 51 μs	25	479 ± 26 μs
QD2	fpt	450	482 + 41μs	65	143 ± 34 μs	35	363 ± 15 μs
QD3	fpt	450	578 ± 111 μs	69	166 ± 51 μs	31	386 ± 106 μs
QD1	air	850	537 ± 14 ns	100	–f	–	537 ± 14 ns
QD2	air	850	401 ± 4 ns	100	–f	–	401 ± 4 ns
QD3	air	850	430 ± 5 ns	100	–f	–	430 ± 5 ns
QD1	fpt	850	270 ± 11 μs	62	60 ± 10 μs	38	190 ± 16 μs
QD2	fpt	850	203 ± 8 μs	60	57 ± 15 μs	40	145 ± 11 μs
QD3	fpt	850	101 ± 5 μs	100	–g	–	101 ± 5 μs

[a] Toluene solution.

[b] Relative contribution to the biexponential fit.

[c] Weighted average lifetime, calculated as $\tau_{avg} = (A_1\tau_1 + A_2\tau_2)/100$.

[d] 95% Confidence interval.

[e] Freeze–pump–thawed samples ($< 10^{-5}$ torr).

[f] Due to instrumental limitations, the fast component could not be resolved and the data was fit to a monoexponential decay.

[g] A biexponential fit was found to be an overparameterization of the data and was thus fit to a monoexponential decay.